AMPEROMETRIC ENZYME ELECTRODES WITH CONDUCTING ORGANIC SALTS AS ELECTRODE MATERIALS

BY

KEVIN MCKENNA

A DISSERTATION PRESENTED TO THE GRADUATE SCHOOL
OF THE UNIVERSITY OF FLORIDA IN
PARTIAL FULFILLMENT OF THE REQUIREMENTS
FOR THE DEGREE OF DOCTOR OF PHILOSOPHY

UNIVERSITY OF FLORIDA

1987

The work contained in this dissertation represents the attainment of a goal which would have been exceedingly difficult without the love and encouragement of my wife, Carol, and my daughters, Erin, Lindsey and Meghan. It is to them and to their understanding that I dedicate this dissertation.

ACKNOWLEDGMENTS

Any author has many debts to colleagues and teachers who have aided and guided him along the way. In this regard, I would like to express my gratitude to Dr. Anna F. Brajter-Toth for her direction and encouragement of my work. I would also like to acknowledge Drs. James D. Winefordner, Gerhard Schmid and John G. Dorsey for their guidance as teachers.

I would like to thank all my friends and colleagues, especially Liakat Bodalbhai and Michael Gehron, for their friendship. In particular, I thank Michael S. Lee for his friendship, encouragement and advice when it was needed.

The support by Merck-Dohme through a fellowship from May, 1986, to May, 1987, is gratefully acknowledged. I am also grateful for the summer fellowship sponsored by the Dow Chemical Company and administered by the Division of Analytical Chemistry of the American Chemical Society.

TABLE OF CONTENTS

LIST OF TABLES

LIST OF FIGURES

Abstract of Dissertation Presented to the Graduate School
of the University of Florida in Partial Fulfillment of the
Requirements for the Degree of Doctor of Philosophy

AMPEROMETRIC ENZYME ELECTRODES WITH
CONDUCTING ORGANIC SALTS AS ELECTRODE MATERIALS

BY

KEVIN MCKENNA

December, 1987

Chairperson: Anna F. Brajter-Toth
Major Department: Chemistry

The purpose of this research was to investigate the behavior of immobilized enzyme electrodes using the conducting organic salts: tetrathiafulvalene tetracyanoquinodimethane, TTF-TCNQ, and N-methylphenazine tetracyanoquinodimethane, NMP-TCNQ, as electrode materials. Tetrathiafulvalene tetracyanoquinodimethane was used as the electrode material in membrane electrodes for the flavoenzymes: xanthine oxidase and oxalate oxidase. The response of the xanthine oxidase membrane electrode to the biological purines: xanthine, hypoxanthine and purine was evaluated in phosphate buffer and in blood plasma. In phosphate buffer, a substrate-dependent current response is linear in the concentration range 2×10^{-5} to 6×10^{-4} M. In comparison, the plasma matrix causes a decrease in the sensitivity and linear dynamic range of the membrane electrode.

Kinetic analysis indicates that the xanthine oxidase membrane electrode operates under membrane mass transport control. For the

above substrates, the effective Michaelis-Menten constants, K_{ME}, are considerably larger than the reported K_M values for the homogeneous enzymatic reactions.

The response of a TTF-TCNQ oxalate oxidase amperometric membrane electrode was also investigated. Results indicate that oxalate oxidase does not react at the TTF-TCNQ electrode.

The behavior of a nicotinamide adenine dinucleotide, NAD, dependent glucose dehydrogenase membrane electrode utilizing NMP-TCNQ and TTF-TCNQ as electrode materials was evaluated for glucose detection. At a bare NMP-TCNQ electrode, a NADH-dependent current is linear in the concentration range 7.5×10^{-5} to 5.0×10^{-4} M. The precision of the response was found to decrease with increasing NADH concentration. In comparison, the response of NADH at a TTF-TCNQ electrode showed increased reproducibility, but decreased sensitivity. A TTF-TCNQ glucose dehydrogenase membrane electrode showed no response in the presence of glucose.

The electrochemical behavior of xanthine, uric acid, 6-mercaptopurine, 6-thioxanthine, dopamine and ascorbate at bare TTF-TCNQ electrodes was evaluated and compared to that observed at rough pyrolytic graphite electrode, RPGE. The reactivity of these compounds at TTF-TCNQ is generally lower than at RPGE. The use of TTF-TCNQ as an electrode in analytical studies is addressed.

CHAPTER 1
INTRODUCTION

1.1 Background

Electrochemical methods are used in a wide variety of laboratory settings. These methods offer the advantages of operational simplicity and low cost instrumentation. The speed and low sample volume requirements of electroanalytical techniques have long been exploited in clinical laboratories (1,2, pp. 94-97). Detection limits have been reported in the ng/mL range using such techniques as differential pulse polarography, square wave voltammetry and anodic stripping voltammetry (3-5). Miniaturization of electrodes has given rise to in vivo measurement of neurotransmitters in the brain and even individual nerve cells (6,7). Recently, electrochemical sensors have seen increased application as liquid chromatographic detectors and have been used in process stream analysis (8).

However, despite the reported success of these methods, electrochemistry, as with most measurement tools, has specific shortcomings that limit its analytical usefulness. The major one among these is the electrode surface which can be fouled by unwanted adsorption processes. This can lead to electrode passivation and concomittant poor precision. In addition, to overcome slow electrochemical reaction rates of some species, the application of a large overpotential is required to cause the desired reaction to

occur. This results in poor sensitivity and, if other electroactive species are present that can react at the applied potential, in poor selectivity. In the past decade, there has been a tremendous amount of research into ways of controlling the nature of the electrode surface as a means of increasing the sensitivity and selectivity of electroanalytical techniques (9,10). One approach taken in this direction is the development of immobilized enzyme electrodes (11, pp. 254-311, 12). Immobilized enzyme electrodes offer the possibility of improving the selectivity of electroanalytical methods while providing the desired sensitivity. This is possible because of the electrode design in which the immobilized enzyme reacts selectively with analytes in a catalytic reaction. The use of enzymes can solve the primary problem of most analytical measurements, the analysis of one substance in the presence of many similar compounds that may interfere in the analysis. Eliminated, therefore, is the need for extensive sample pretreatment. Moreover, by physically confining the enzyme at the electrode surface, the enzyme can be repeatedly used, thereby greatly reducing the cost of analysis relative to the selective homogeneous assay.

An enzyme-based electrode is illustrated in Figure 1-1. The operation of this device is based on diffusion-controlled movement of substrate through a thin layer of enzyme (1). The substrate reacts with the enzyme to form a product which is detected at the electrode surface (1,13). Although the basic concept is the same for both amperometric and potentiometric enzyme electrodes, there are substantial differences between the two devices. In the

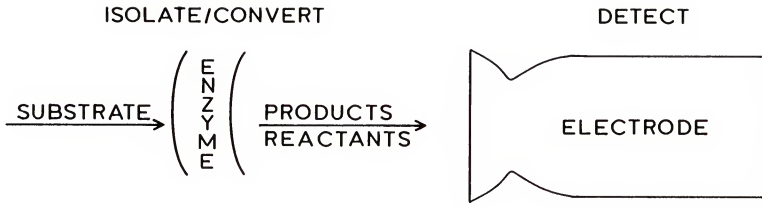

Figure 1-1. Enzyme-based electrode.

potentiometric type, a change in potential at a sensing surface is measured that is proportional to the logarithm of the analyte concentration (activity) (13,14). Potentiometric measurements are made under conditions of essentially zero current flow. The advantages of potentiometric enzyme electrodes are the simplicity of operation and their low cost. However, they are not without shortcomings. The Nernstian slope for an ideal univalent potentiometric electrode is 0.059 V/decade at 25°C (11, p. 220, 14). Thus, the electronics of the sensing system must be able to reproducibly distinguish between small voltage differences. It has been reported that the majority of potentiometric enzyme electrodes show a less than ideal Nernstian response (13). This means frequent calibration of these devices is required (14). An additional limitation is their restricted linear dynamic range (13). Moreover, there are few enzyme systems compatible with the operation of these electrodes (e.g., producing CO_2 or NH_3 in the enzymatic reaction) (11, p. 200, 13,14).

With amperometric enzyme electrodes a voltage is applied between the working and reference electrodes. This applied potential gives rise to an electron transfer reaction, causing a current flow that is proportional to the concentration of the analyte (1,13,15,16). Higher sensitivity and wider linear ranges have been reported for amperometric enzyme electrodes relative to their potentiometric counterparts (13,15,16). The major advantage of amperometric detection is that it is compatible with a larger number of enzyme systems. For example, Clark listed twenty-seven flavoenzymes that

produce hydrogen peroxide or use oxygen as an electron acceptor in the enzymatic reaction (17, p. 377). Both hydrogen peroxide and oxygen can be detected amperometrically.

In the original design, analysis with amperometric enzyme electrodes relied on the detection of the endproduct of the enzymatic reaction (11, p. 118, 12). For continuous operation of electrodes with immobilized flavoenzymes, an acceptor was required which regenerated the enzyme following the enzyme-analyte reaction. In a newer design, the analytical signal was produced when the acceptor was regenerated electrochemically, acting as a mediator between the electrode and the enzyme (18-20). The success of the mediated reaction relied on the choice of the mediator, which had to rapidly react with the enzyme and the electrode at moderate potentials.

In the simplest design, the analytical signal would be obtained as a result of a direct regeneration of the enzyme at the electrode surface following the enzyme-analyte reaction. The success of this approach lies in the choice of electrode material. Recently, it has been reported that the reduced flavin adenine dinucleotide redox center ($FADH_2$) of flavoenzymes undergoes direct oxidation at conducting organic salt electrodes (21-24). The main thrust of these reports has been the development of the general theory of these types of unmediated amperometric enzyme electrodes. The main objective of this research was the development of amperometric immobilized enzyme electrodes constructed with the conducting organic salts tetrathiafulvalene tetracyanoquinodimethane, TTF-TCNQ, and

N-methylphenazine tetracyanoquinodimethane, NMP-TCNQ, as the electrode material.

Recently, we reported on the use of electrochemistry, in conjunction with other analytical methods, in the investigation of the electrooxidation and enzymatic oxidation of 6-thioxanthine, 6-TX (25). It was also of interest to develop a simple method for the detection of 6-TX and/or its parent compound 6-mercaptopurine, 6-MP. Due to its ability to catalytically oxidize 6-TX and 6-MP (26) and its low electron acceptor specificity (18,20,27, p. 110), xanthine oxidase was chosen as the flavoenzyme to be used in the construction of an amperometric enzyme electrode for the measurement of the thiopurines. In addition to thiopurines, xanthine oxidase catalytically oxidizes the biological purines: xanthine, hypoxanthine and purine (28, p. 318). The determination of these purines are also of analytical interest, and their measurement was undertaken as part of this study.

It was also of interest to evaluate the response of the TTF-TCNQ salt to a flavoenzyme of high electron acceptor specificity. Oxalate oxidase is a flavoenzyme recognized as having high acceptor specificity, exchanging electrons only with oxygen in homogeneous solutions (20,29). Because the analytical usefulness of determining oxalic acid in body fluid is well-documented (2, p. 185, 30), an oxalate oxidase amperometric enzyme was constructed using the conducting organic salt TTF-TCNQ and its response in the presence of oxalic acid was investigated.

The enzyme cofactor nicotinamide adenine dinucleotide, NAD, makes up one of the two main classes of redox coenzymes that function in simple enzyme-catalyzed dehydrogenation (31). About 300 dehydrogenases are known to require NAD as a cofactor, producing the reduced form NADH in the catalytic reaction (32, p. 401). There has been increasing interest in recent years in the electrochemical oxidation of NADH because electrochemical methods of coenzyme regeneration may provide an economical means for the synthesis and determination of a variety of important biological compounds (33-37). In this work, conducting organic salts were evaluated as electrode materials in electroanalytical studies involving NADH oxidation. The electrode materials to be investigated were NMP-TCNQ and TTF-TCNQ. N-Methylphenazine tetracyanoquinodimethane was chosen as an electrode material for two reasons: 1) NMP has been shown to exchange electrons with NADH in homogeneous aqueous solutions and 2) Albery and coworkers have reported that NADH reacts at NMP-TCNQ electrodes (37-39). As of yet, no work has been reported in exploiting the electroanalytical potentials of this salt. Research was also undertaken to construct an immobilized enzyme electrode using a NAD-dependent enzyme. Glucose dehydrogenase was chosen as the enzyme to be studied. The substrate (glucose) and the product of the enzymatic reaction (gluconolactone) are both electrochemically inactive.

A major concern in electroanalytical measurements is the rate of heterogeneous charge transfer. When the rate is small, electroanalytical measurements are difficult, and it is of

considerable interest to be able to control the electrode surface as a means of increasing the electrochemical reaction rate. One means of accomplishing this is the use of novel electrode materials that can possibly enhance the rate of electrode reactions (9,10). The focus of this portion of this research deals with evaluating the reactivity of biological molecules at a TTF-TCNQ electrode. The applicability of this salt as an electrode material in measuring these compounds will be discussed. In addition, the results obtained at the TTF-TCNQ electrode are compared to those obtained at a rough pyrolytic graphite electrode, RPGE, which is considered an active surface (i.e., fast electrode surface).

1.2 Organic Conducting Salts

In 1960, Melby and coworkers described the new powerful electron acceptor 7,7,8,8 tetracyanoquinodimethane, TCNQ, Figure 1-2 (40). This compound was the first stable organic material which could conduct electricity like a metal. The preparation (41) of a new donor, tetrathiafulvalene, TTF, Figure 1-2, led to the discovery that the chloride salt of TTF had high conductivity (42) (σ_{RT} 0.2 (ohm cm)$^{-1}$). In 1973, the complexes of TTF (43) and N-methylphenazine, NMP (44), Figure 1-2, with TCNQ were both found to be metallic at room temperature (σ_{RT} 500 and 200 (ohm cm)$^{-1}$, respectively). Since then hundreds of different molecular complexes containing TCNQ have been made (45-48). The high conductivity arises because in the crystalline compound the large planar molecules can stack on top of each other with considerable pi (π) electron overlap

DONORS:

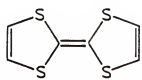

Tetrathiafulvalene,(TTF)

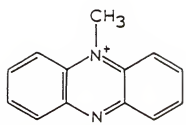

N-Methylphenazine,(NMP)

ACCEPTOR:

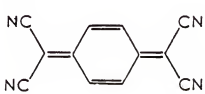

Tetracyanoquinodimethane,(TCNQ)

Figure 1-2. Structures of components of conducting organic salt complexes.

and delocalization (45). The transferred charge can move easily along separate donor and acceptor stacks giving rise to anisotropic (1-D) conductivity (45,47) because the π-orbital overlap is greater along the stacks than in other directions. The most extensively studied complex is TTF-TCNQ because its preparation is relatively simple (45). Certain key features of TTF and TCNQ make them stand out over other donors and acceptors. Both molecules are of similar size, both are planar with delocalization extending throughout the molecule, both have the same high degree of symmetry (D_{2h}); and the ionization potential/electron affinity values for the pair favor incomplete charge transfer (45,47).

Much of the current interest in conducting organic salts has stemmed from their technological potential (e.g., as lightweight electrodes). These materials are also of interest as electrodes for electroanalytical studies. Jaeger and Bard reported on the behavior of various donor-TCNQ complexes as electrodes (49,50). The results show that the electrodes have a stable region where they behave as inert electrodes capable of carrying out electrochemical reactions of dissolved solutes. Outside this region different reactions of the electrodes occur which depended on the nature of the supporting electrolyte.

Bard et al. have described the preparation and the properties of a bioconductive polymer in which TTF was incorporated into a perfluorinated sulfonate polymer, Nafion (51). Kaufman et al. examined the electrochemical behavior of TCNQ-polyester coated electrodes in order to gain an understanding of the nature of these

polymer films (52-55). Chambers and coworkers investigated the behavior of TCNQ-polyester thin films (56-58).

1.3 Biological Significance of Analytes Studied

1.3.1 Purines

Nucleic acids, nucleotides and nucleosides contain heterocyclic bases of two classes: the pyrimidines and the purines (59). The purine ring system can be viewed as a pyrimidine fused to an imidazole (32, p. 323). The Beilstein convention is used in numbering the purines, Figure 1-3A (59). The two most important purines are adenine and guanine, Figures 1-3B and 1-3C, respectively. The purines xanthine, hypoxanthine and uric acid, Figures 1-3D, 1-3E and 1-3F, respectively, are important metabolites but are far less abundant than adenine and guanine (32, p. 324). The biosynthesis of the purine ring is driven by the hydrolysis of seven phosphoanhydride bonds (32, p. 955). Hence, molecules containing the purine ring are too important to burn as fuel, and most organisms contain pathways to salvage these molecules (32, p. 955). If not salvaged and reused, the free purines are degraded to the endproduct uric acid by the flavoenzyme xanthine oxidase (26).

The degradation of purines to uric acid in man has been intensively studied since genetic aberrations of this pathway are known (59, p. 740). Gout is an extremely painful condition whose major biochemical symptom is excess production of uric acid. Deficiency in one of the salvage pathways results in Lesch-Nyhan

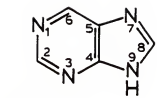

A. Purine

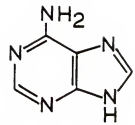

B. Adenine

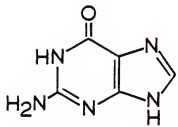

C. Guanine

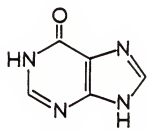

D. Hypoxanthine

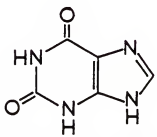

E. Xanthine

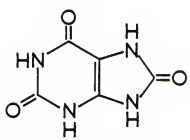

F. Uric Acid

Figure 1-3. Structures of purines.

syndrome in inheritable metabolic disease (32, p. 956). In this genetic disorder, there is a deficiency in the enzyme guanine (hypoxanthine) phosphoribosyltransferase, and guanine and hypoxanthine are not salvaged (59, p. 740). The result is an excess production of uric acid. In patients with congenital xanthine oxidase deficiency (xanthinuria), blood and urine concentrations of hypoxanthine and xanthine are increased and uric acid levels are decreased (2, p. 624). Therefore, it is necessary to determine the concentration of purine, hypoxanthine and xanthine in blood fluids when xanthine oxidase inhibitors are administered as well as in patients with the above congenital enzyme defects.

Several analytical approaches have been reported for measuring oxypurines (hypoxanthine and xanthine) in body fluids. They include spectrophotometric (60,61), chromatographic (62-64), mass spectrometric (65, p. 209, 66) and electrochemical methods (18,19). Spectrophotometric methods required extensive sample pretreatment and as a result was tedious and time-consuming. The chromatographic method although sensitive suffered from extensive sample pretreatment requirements. Mass spectrometry is a sensitive tool, but quantitation is difficult. Yacynych and coworkers employed a chemically modified graphite electrode containing covalently immobilized xanthine oxidase for the detection of xanthine (18). Potassium hexacyanoferrate (III) was used as the electron acceptor in the enzyme-catalyzed reaction. High solubility of the acceptor in aqueous solution prevented it from being effectively trapped in the enzyme layer.

1.3.2 Oxalate

Measurement of oxalic acid in biological fluids is of clinical interest because it has been estimated that two-thirds of all kidney stones and over three-fourths of endemic bladder stones contain calcium oxalate (67). The food industry is also interested in oxalate determination. Calcium oxalate crystal formation in finished beer gives rise to haze or to extensive formation of carbon dioxide (68).

Current methods for the determination of oxalate can be divided into four groups: 1) direct precipitation (69-71); 2) solvent extraction (72-74); 3) isotope dilution (68,75); and 4) enzymatic methods (76-79). The direct precipitation of oxalate as its calcium salt (solubility 0.58 mg/dL) followed by permanganate titration or colorimetric detection with indole has been described (69,70). The use of europium instead of calcium for the precipitation of oxalate has been reported (71). The europium is detected by polarography. The precipitation methods were tedious, time-consuming and suffered from interference by other body fluid constituents. These interferences can be decreased by first extracting the oxalate with diethyl ether (72,73). Improvements in specificity have been achieved, usually at the expense of increasing the complexity of the procedure (74). The use of C-labelled oxalic acid to check the recovery of oxalic acid has been reported (68,75). However, the isotope dilution method is very labor intensive and is not suitable as a routine method.

The most specific method appears to be the enzymatic approach. Spectrophotometric methods utilizing either the enzyme oxalate decarboxylase (EC 4.1.1.2) or oxalate oxidase (EC 1.2.3.4) have been described (76,77), but these methods suffer the disadvantages of homogeneous enzyme assays. Kobos and Ramsey immobilized oxalate decarboxylase on the tip of a carbon dioxide sensing electrode (78). Guilbault and coworkers constructed an immobilized oxalate oxidase on pig intestine, mounted on the tip of an oxygen sensor (79). These devices are relatively complicated and suffer from long response times.

1.3.3 Thiopurines

Azathiopurine (6-(1-methyl-4-nitroimidazol-5-ylthiopurine), Figure 1-4A, is an antineoplastic agent used in cancer patients for remission induction and consolidation and maintenance therapy of acute leukemias (80). It has also found use as an immunosuppressive agent for patients undergoing organ transplantation (80). The active form of azathiopurine is the metabolite 6-mercaptopurine, 6-MP, Figure 1-4B (81, p. 812). 6-Mercaptopurine competes with hypoxanthine and guanine for the enzyme hypoxanthine-guanine phosphoribosyltransferase and is itself converted to thioinosinic acid (TIMP) (81, p. 812). This intracellular nucleotide inhibits several reactions involving inosinic acid (IMP) including the conversion of IMP to adenylic acid (AMP) via adenylosuccinate. Thioinosinic acid has been reported to inhibit glutamine-5-phosphoribosylpyrophosphate amidotransferase, the first enzyme unique to the de novo pathway for purine ribonucleotide synthesis (80).

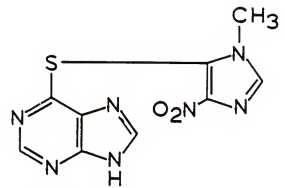

A. Azathioprine

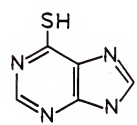

B. 6-Mercaptopurine

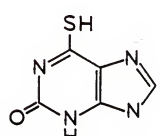

C. 6-Thioxanthine

Figure 1-4. Structures of 6-thiopurines.

6-Mercaptopurine is also catalytically oxidized by xanthine oxidase to form 6-thioxanthine, 6-TX, Figure 1-4C.

Although it is likely that biological effects correlate better with intracellular 6-MP concentrations than with plasma concentration of unmetabolized 6-MP, it would be helpful to investigate 6-MP concentration as a function of time versus biological effects (82). In light of 6-MP bone marrow toxicity, hepatotoxicity and carcinogenicity monitoring 6-MP plasma concentrations can also be helpful for the study of interactions of other drugs with this agent and dosage adjustments in patients with impaired organ function (80).

Numerous approaches have been described for the detection of azathiopurine and its active metabolite 6-MP. One of the first sensitive methods was based on spectrofluorometric detection of its oxidation product purine-6-sulfonate (83). Although this method was sensitive, it suffered from interferences. Wong and Maddocks (84) described a thin-layer electrophoretic method to separate thiopurine derivatives but the method was qualitative at best. Floberg et al. developed a procedure to detect 6-MP using gas chromatography/mass spectrometry, GC/MS (85). It was shown that GC/MS was a sensitive tool for the assay of 6-MP. However, the need to use MS has prevented its wide application in routine analysis. Several reversed phase liquid chromatographic procedures have been described for measuring 6-MP in human plasma (81,86). These methods involve extensive sample pretreatment and suffer from long turn-around times.

1.3.4 Nicotinamide Adenine Dinucleotide

Nicotinamide adenine dinucleotide (NAD) is composed of an AMP moeity in phosphodiester linkage to a 5 phosphoribosyl-1-nicotinamide, Figure 1-5 (87). The portion of the molecule that is redox active is the nicotinamide ring system (32, p. 401). The oxidized pyridinium system of NAD can accept two electrons reversibly to give a dihydropyridine ring (31). Two electron reduction involves the addition of one hydrogen to form the dihydropyridine ring. The 1,4 dihydropyridine is the exclusive isomer found biologically (32).

The rate or amount of NADH production is used in a wide variety of systems to assay the enzyme activity or the concentration of the enzymes' substrate concentration, respectively (2, p. 354). There has been increasing interest in recent years in the electrochemical oxidation of NADH (33-37). Such measurements incorporating NAD are currently performed using spectrophotometric methods (2, p. 354, 38).

The electrochemistry of NADH has been excellently reviewed (88). It proceeds irreversibly at all known solid electrodes. At platinum and carbon electrodes, at pH 7.0, the overvoltage is about 1 volt (89,90). Only a few redox couples can exchange electrons with NADH in a homogeneous aqueous solution and they include flavins (91), phenazines (92), phenathiazines (92) and 1,2 quinones (93). Intentional immobilization of molecules on electrodes results in what is referred to as chemically modified electrodes, CME (9). Such electrodes have proved useful as a means for bringing about specific electrocatalytic reactions (10). Attempts, therefore, have been made to use some of the above molecular structures to construct CME in

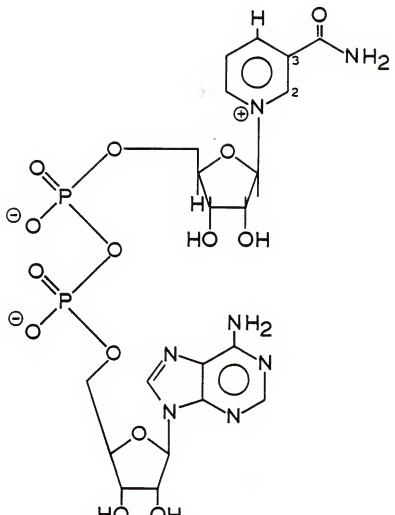

Nicotinamide Adenine Dinucleotide

Figure 1-5. Structure of the enzyme cofactor nicotinamide adenine dinucleotide.

order to speed up the heterogeneous electron transfer between the electrode and NADH in solution. Tse and Kuwana immobilized quinones onto a graphite electrode (93). The immobilized quinones showed catalytic activity, and the overpotential was lowered by 200 mV. However, the electrode lost its activity after a few cycles. Degrand and Miller reacted dopamine, with a 1,2 quinone functionality with poly(methacryoyl chloride) to form a polymer which was immobilized onto carbon electrodes (36). The decrease in overvoltage was the same as reported by Tse and Kuwana (93), and the electrode suffered from poor stability. Gorton and coworkers adsorbed phenazines on the surface of graphite and platinum electrodes (92). The overpotential was reduced 550 mV compared to bare graphite and 700 mV relative to bare platinum. However, electrode stability again proved to be troublesome; activity decreased 80% in 15 hours. Albery and Bartlett have reported that NADH oxidation is catalyzed at a NMP-TCNQ electrode (37). The apparent heterogeneous rate constant of 10^{-3} cm s^{-1} has been reported for NADH oxidation under the assumption of Langmuirian adsorption of the reactant. The response of NADH at organic metal-like electrodes as a function of concentration has not been previously reported.

1.4 Enzyme Systems

1.4.1 Xanthine Oxidase

Xanthine oxidase (EC 1.1.3.2) is one of the most studied and complex flavoenzymes (94). It has been purified to homogeneity from buttermilk and other sources (87, p. 432). The buttermilk enzyme is

a dimer of 260,000 molecular weight (32, p. 952). Each such unit has one molecule of flavin adenine dinucleonite, FAD, and one molecule of Mo(IV). There are also four atoms of iron and an equivalent amount of inorganic sulfide (87, p. 433). Xanthine oxidase is recognized to be an enzyme of low specificity catalyzing the oxidation of purines, pyrimidines and azathiopurines (95, p. 443). Moreover, its acceptor specificity is also low; in addition to molecular oxygen, cytochrome c (94), ferrocyanide (18), ferrocene derivatives (20) and artificial dyes (95, p. 443) can serve as electron acceptors. The enzyme is capable of taking up to six electrons (two at the molybdenum, two at the FAD and one each at the two iron-sulfur centers) (95, p. 443) There is electron transfer within the enzyme; the electrons enter the enzyme at the Mo(VI) ion and exit to oxygen at the $FADH_2$ molecule (87, p. 433). The stoichiometry of the xanthine oxidase reaction suggests oxidation of an aldehyde by two electrons with introduction of a hydroxyl group from water into the product at the oxidation site.

1.4.2 Oxalate Oxidase

Oxalate oxidase (EC 1.2.3.4) is a flavoenzyme which catalyzes the aerobic oxidation of oxalic acid:

$$(COOH)_2 + O_2 \xrightarrow[\text{oxidase}]{\text{oxalate}} 2\ CO_2 + H_2O_2$$

This enzyme is found in mosses and higher plants (29,96). The molecular weight is 150,000, and it consists of two identical subunits (97,98). Oxalate oxidase is an enzyme of high specificity

having high activity towards oxalic acid but none towards other acids (97). In addition, reduced oxalate oxidase exchanges electrons only with molecular oxygen in homogeneous solution. It has been reported that 2,6 dichlorophenolindophenol, phenothiazine methosulfate, methylene blue, ferrocyanide and ferrocene derivatives were not effective as electron acceptors under anaerobic conditions (29,97,99). The oxalate oxidase isolated from barley seeds is activated by 8-hydroxyquinoline (29,77) and is inhibited by nitrate, halogens and sodium azide (97). The enzyme shows greatest activity at pH 3.5 and is very stable in the acidic pH range from pH 2 to pH 4 (97,98).

1.4.3 Glucose Dehydrogenase

Glucose dehydrogenase (EC 1.1.1.47) catalyzes the direct oxidation of glucose to gluconolactone utilizing as a coenzyme either nicotinamide adenine dinucleotide, NAD, or nicotinamide adenine dinucleotide phosphate, NADP. The catalytical reaction is shown below.

$$\text{B-D-glucose} + \text{NAD(P)} \xrightarrow[\text{dehydrogenase}]{\text{glucose}} \text{gluconolactone} + \text{NAD(P)H}$$

The enzyme has been isolated from liver homogenates of species representing five vertebrate orders (27, p. 70). The hepatic enzyme has a molecular weight of 230,000 and is highly specific for β-D glucose (100). The Michaelis constant, K_M, value (that substrate concentration that gives one-half maximum velocity) for glucose dehydrogenase depends on the enzyme source and varies from 0.06 to

1.7 M (27, p. 71, 100). The optimum reaction pH also depends on the source of the enzyme and varies from pH 7.7 to pH 8.3 (100). Glucose-6-phosphate, fructose 1,6-phosphate, ribose 5-phosphate, and fructose 6-phosphate have been reported to inhibit glucose dehydrogenase (101-103).

1.5 Electrochemical Measurements

In cyclic voltammetry, a potential, in a triangular waveform, is applied to a working electrode which is immersed in a quiescent solution. The potential of the working electrode is controlled versus a reference electrode (e.g., a saturated calomel electrode, SCE). Cyclic voltammetry is often the first experiment performed in an electrochemical study because it provides a rapid means to characterize redox systems (104, p. 86).

The important parameters in cyclic voltammetry are the anodic and cathodic peak current (i_{Pa} and i_{Pc}, respectively) and the anodic and cathodic peak potentials (E_{Pa} and E_{Pc}, respectively). An electrochemically reversible system is one in which electron transfer is mass transfer limited, $K_s > 1$ cm s^{-1} (105). In such systems, the difference in peak potentials, ΔE_p, is given by equation 1.1 (26, pp. 90-92):

$$\Delta E_P = E_{Pa} - E_{Pc} = \frac{0.059}{n} \qquad \text{eq. 1.1}$$

where n is the number of electrons/mole and the peak potentials are measured in volts. The ratio of anodic to cathodic peak current

values for a reversible couple is given in equation 1.2 (104, pp. 90-92).

$$\frac{i_{Pa}}{i_{Pc}} = 1 \qquad \text{eq. 1.2}$$

Electrochemical irreversibility is characterized by a K_s value of less than 10^{-3} cm s^{-1} (105). In cyclic voltammetry, a peak potential difference greater than 0.059/n volts and a i_{Pa}/i_{Pc} ratio of less than one are observed (104, pp. 90-92).

Cyclic voltammetry is also useful for differentiating between diffusion and adsorption controlled processes (106, pp. 218-222, 522-525). For a model reaction,

$$O + ne \rightleftharpoons R \qquad \text{eq. 1.3}$$

occurring under diffusion, O undergoes reduction at the electrode surface to form R with a resultant depletion of O at the electrode surface. A concentration gradient is created causing a diffusional mass transfer of O from an area of high concentration (bulk solution) to an area of low concentration (electrode surface). In an adsorption controlled process, O and/or R interact with the electrode through hydrophobicity of the adsorbant, electrostatic attraction or adsorbant-electrode bonding, and are accumulated at the electrode (26, pp. 43-49). Equations 1.4 and 1.5 describe the peak current for a reversible and irreversible diffusion controlled processes, respectively (106, pp. 218-222).

$$i_p = (2.65 \times 10^5)\, n^{3/2}\, AD_o^{1/2}\, v^{1/2}\, C_o^* \qquad \text{eq. 1.4}$$

$$i_p = (2.99 \times 10^5)\, n(\alpha n_a)^{1/2}\, AC_o^*\, D_o^{1/2}\, v^{1/2} \qquad \text{eq. 1.5}$$

Equations 1.6 and 1.7 describe the peak current for a reversible and irreversible adsorption controlled processes, respectively (106, pp. 522-525).

$$i_p = \frac{n^2 F^2}{4RT}\, v\, A\, \Gamma_o^* \qquad \text{eq. 1.6}$$

$$i_p = \frac{n\alpha n_a F^2\, A\, v\, \Gamma_o^*}{2.718\ RT} \qquad \text{eq. 1.7}$$

where n is the number of electrons per molecule oxidized or reduced; A is the electrode area (cm^2); D_o is the diffusion coefficient ($cm^2\ sec^{-1}$); v is the scan rate (V/sec); C_o is the concentration of oxidizable species (M); α is the transfer coefficient; n_a is the number of electrons in the rate-limiting step; F is Faraday's constant (96,486 coulombs per mole of electrons); R is the gas constant (8.314 J mol^{-1} K^{-1}); T is temperature (K); and Γ_o^* is the surface excess of species O at equilibrium. The plot of log i_p versus log v enables the differentiation between the diffusion and adsorption controlled processes.

A potentiostat allows the potential of a working electrode to be controlled with respect to a reference electrode (106, p. 136). This is done in a three-electrode electrochemical cell by applying a

voltage to the auxiliary electrode. The potentiostat adjusts this voltage to maintain the programmed potential between the working and reference electrodes. The potential difference between these two electrodes is sensed through a high-impedance feedback loop (106, p. 136).

To induce a redox reaction, the selection of the correct constant potential to be applied to the working electrode is made by examining a voltammogram of the redox system (104, pp. 119-121). The applied potential should be applied as to maximize the signal to noise ratio of the measurement (i.e., in the potential region of the maximum reaction rate).

CHAPTER 2
EXPERIMENTAL

2.1 Materials

The enzymes: xanthine oxidase from buttermilk (EC 1.1.3.2) grade III, activity 1.1 units/mg; oxalate oxidase from barley seeds (EC 1.2.3.4), activity 0.5-1.5 units/mg; glucose oxidase from Aspergillus species (EC 1.1.3.4), activity 100,000-150,000 units/mg; and glucose dehydrogenase from Bacillus species (EC 1.1.1.47), activity 200 units/mg were obtained from Sigma. The coenzymes, β-nicotinamide adenine dinucleotide (β-NAD) grade III and β-nicotinamide adenine dinucleotide, reduced form (β-NADH) grade III, were also obtained from Sigma. The TTF and NMP (as the methosulfate salt) were purchased from Aldrich as was the TCNQ. All other chemicals were reagent grade and were used as received. All solutions were prepared using doubly-distilled water. Experiments in which NMP-TCNQ electrodes were used were carried out in 0.1 M Tris-HCl buffer, pH 7.0. Experiments in which TTF-TCNQ electrodes were used were performed in either phosphate buffers, ionic strength 0.5 M or pH 3.5 succinate buffer, ionic strength 0.05 M. Single-donor blood bank plasma (North Florida Regional Medical Center, Blood Bank Department) was used to prepare stock solutions of purine and hypoxanthine. Working solutions were prepared by diluting the stock solution with the plasma. Ascorbate, NAD, NADH and dopamine

solutions were prepared fresh daily, and care was taken to protect these solutions from the light. Solutions were deaerated by bubbling N_2 through the solutions for at least 10 minutes prior to electrochemical measurements.

2.2 Apparatus

Direct current cyclic voltammetry and constant potential experiments were performed with a Bioanalytical Systems Electrochemical Analyzer, BAS-100, and a Houston Instruments DMP-40 series digital plotter. All experiments were carried out with the conventional three-electrode system using a saturated KCl-agar salt bridge. All potentials were measured and are reported versus a saturated calomel electrode (SCE) which was prepared in this laboratory. In addition to the working and reference electrodes, the cell contained a 1-cm^2 platinum foil counter electrode. Rough pyrolytic graphite electrodes (RPGE) were prepared by sealing a 0.02 cm^2 piece of pyrolytic graphite (Pfizer) into the end of a glass tube with inert epoxy (Epoxi-Patch, Dexter Corp.). Electrical contact was made to the rear of the electrode surface with a few drops of mercury and a copper wire. The electrodes were resurfaced (roughened) before each experiment by polishing on a Ecomet I polisher-grinder (Buehler Inc.) with 600-grit silical carbide paper. The temperature of the solutions was thermostatically maintained using a YSI model 172 proportional temperature controller.

2.3 Organic Salt Preparation

2.3.1 Tetrathiafulvalene Tetracyanoquinodimethane

The TTF-TCNQ complex was synthesized by mixing equimolar (0.1 M) hot anhydrous acetonitrile (Fisher) solutions of neutral TTF and TCNQ (49). The black complex immediately precipitated as a microcrystalline powder. The solution was allowed to come to room temperature while mixing. The precipitate was collected using vacuum filtration and washed five times with cold acetonitrile. The precipitate was then washed five times with cold diethyl ether (Fisher) and dried under vacuum for 16 hours. Care was taken to protect the complex from light. The dried complex was placed in a darkened vacuum dessicator and refrigerated until used.

2.3.2 N-Methylphenazine Tetracyanoquinodimethane

The NMP-TCNQ complex was prepared by mixing a hot absolute alcohol solution of NMP (0.1 M) with a boiling absolute alcohol solution of LiTCNQ (0.05 M) (107). A black precipitate formed immediately which was allowed to cool to room temperature while mixing. The precipitate was collected using vacuum filtration and washed five times with cold acetonitrile. The precipitate was then washed five times with cold diethyl ether and dried under vacuum for 16 hours. The NMP-TCNQ was recrystallized from acetonitrile, and the above washing and drying was repeated. During the above procedure, care was taken to protect the complex from light. The dried complex was placed in a darkened vacuum dessicator and refrigerated until used.

The LiTCNQ salt was prepared by mixing a hot acetonitrile solution of lithium iodide (Aldrich) (0.3 M), with a hot acetonitrile solution of TCNQ (0.1 M) (40). Purple microcrystals form in a dark brown solution. The solution was allowed to cool to room temperature while mixing. The precipitate was collected using vacuum filtration and washed with cold acetonitrile until the wash was bright green. The precipitate was then washed five times with cold diethyl ether and dried under vacuum. In the preparation of this salt, care was taken to avoid contamination through dirty glassware or stopcock grease. All glassware was acid-washed and rinsed in doubly-distilled water. A minimum of stopcock grease was used for the glassware joints. The dried salt was placed in a darkened vacuum dessicator and refrigerated until used.

2.4 Conducting Organic Salt Electrodes

The electrodes consisted of a 3.5 mm diameter platinum disk fitted into Telfon holder with a recessed depth of 1.0 mm, Figure 2-1 (23). Contact was made by connecting a copper wire to one side of the disk using conducting epoxy (Tra-con, Medford, MA). The electrode was placed in a 90°C hot air oven to facilitate curing of the epoxy. The cavity was filled with a slurry, a conducting organic salt and polyvinyl chloride (PVC) (13:1, w/w) (23). The slurry was prepared by first dissolving the PVC (Fisher) in tetrahydrofuran (THF) (Fisher) using a watch glass. The conducting organic salt was then added to the dissolved PVC along with an additional 2 mL of THF. The slurry was mixed continuously until it reached the

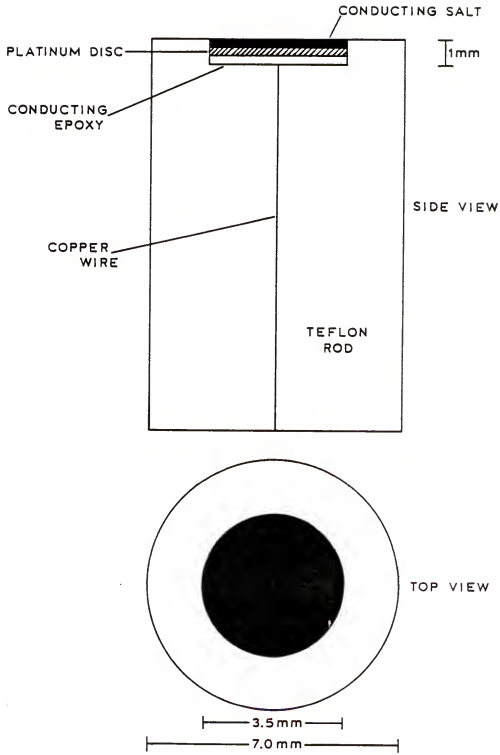

Figure 2-1. Schematic diagram of the conducting organic salt electrode.

consistency of thick honey. At this time it was pressed into the electrode recess using the flat end of a spatula. The electrode was allowed to cure for at least 12 hours in the dark at room temperature, and the excess salt was trimmed off. The electrodes were stored in the dark until ready to use. The resistance of the TTF-TCNQ electrode was typically ca. 50 ohms and that of the NMP-TCNQ was ca. 250 ohms when measured between the electrode surface and the copper wire using a digital voltmeter.

2.5 Preparation of Enzyme Membrane Electrodes

Membrane electrodes were prepared using either porous dialysis tubing, molecular weight cutoff 6,000-8,000 (Spectrapor #1, Spectrum Medical Industries, Los Angeles, CA) or anion exchange membranes (RAI Research Corp.). The dialysis membrane was boiled for 10 minutes in 1% (w/w) Na_2CO_3 (Fisher) to soften the tubing and to remove impurities (23). Four-centimeter squares of the tubing were stored in a solution of 10 mM Tris (Sigma) and 1 mM ethylenediaminetetra-acetic acid, EDTA (Sigma) at 4°C (23). The anion exchange membrane was boiled in 1.0 M HCl and then boiled in 1.0 M NaOH (108). This procedure was repeated three times, rinsing the membranes with doubly-distilled water between boiling. The membrane was stored in 0.1 M Tris-HCl, pH 7.0 at 4°C. Xanthine oxidase was obtained as a suspension in 2.3 M $(NH_4)_2SO_4$ solution. Glucose oxidase was purchased as a solution in 0.1 M, pH 4 sodium acetate buffer. The xanthine oxidase membrane electrode was prepared by trapping 0.050 mL of a 90 μM enzyme suspension at the TTF-TCNQ electrode surface using

a porous dialysis membrane. The glucose oxidase membrane electrode was constructed by trapping 0.050 mL of a 0.10 mM enzyme solution in the same manner. Oxalate oxidase and glucose dehydrogenase were purchased as dry lyophilized powders. Oxalate oxidase was reconstituted using 0.05 M, pH 3.5 succinate buffer. The oxalate oxidase membrane electrode was prepared by immobilizing 0.050 mL of a 56 μM enzyme solution at the TTF-TCNQ electrode surface using a porous dialysis membrane. The buffer used to reconstitute the glucose dehydrogenase depended on the electrode material (0.1 M, pH 7.0 Tris buffer was used for the NMP-TCNQ electrode and 0.5 M, pH 7.0 phosphate buffer was used for the TTF-NCNQ electrode). The glucose dehydrogenase membrane electrode was constructed by coimmobilizing a 37 μM solution of the enzyme with the NAD cofactor at the electrode surface with either a porous dialysis membrane or an anion exchange membrane. The membranes were fixed in place by an O-ring and Teflon tape. Excess enzyme solution was removed by copious washing with doubly-distilled water. The enzyme membrane electrodes were prepared fresh daily. The membrane electrode was placed in supporting electrolyte and deaerated with N_2 for 10 min. prior to electrochemical measurements.

2.6 Electrochemical Measurements

The potential of the TTF-TCNQ electrodes was poised at +0.225 mV versus SCE for 2-3 min. prior to preparing the membrane electrodes on performing cyclic voltammetric experiments. The constant potential experiments were repeated until a stable background current

(25-35 nA) was obtained. At NMP-TCNQ electrodes, the potential was poised at 0.075 mV for 2-3 min. and applied until the current decreased to ca. 5.0 μA. These constant potential experiments were repeated if the background current started to increase (as measured by cyclic voltammetry). Otherwise, this pretreatment of the electrode was only performed before electrochemical measurements or the construction of the enzyme membrane electrode. Figure 2-2A shows a cyclic voltammogram of a TTF-TCNQ electrode obtained in phosphate buffer after electrochemical pretreatment. A cyclic voltammogram of a NMP-TCNQ electrode in 0.1 M, pH 7.0 Tris buffer is shown in Figure 2-2B. These background responses are typical for the organic conducting electrodes in their respective supporting electrolytes for the shown potential windows. As long as the electrodes exhibited this behavior they were used in subsequent electrochemical measurements.

In the construction of the calibration curves using bare TTF-TCNQ electrodes, all current measurements were made at +0.225 mV versus SCE. Cyclic voltammograms were recorded in supporting electrolyte blanks (from -0.05 V to 0.400 V versus SCE) before each cyclic voltammogram of the analyte and the background currents (obtained at 0.225 V) were subtracted from the current values obtained for the analyte. The same procedure was used for the bare NMP-TCNQ electrodes but currents were measured at +0.075 V versus SCE. Before each measurement, the electrode surface was sprayed with a stream of doubly-distilled water and gently dabbed dry with a tissue.

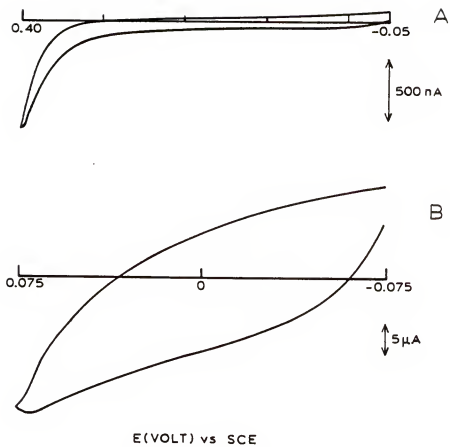

Figure 2-2. Response of electrochemically pretreated organic salt electrodes: (A) TTF-TCNQ in 0.5 M, pH 8.0 phosphate buffer; (B) NMP-TCNQ in 0.1 M, pH 7.0 Tris buffer. Scan rate = 5 mV s, initial sweep to positive potentials, electrode area 0.10 cm^2.

CHAPTER 3
RESPONSE OF IMMOBILIZED FLAVOENZYMES AT TETRATHIAFULVALENE TETRACYANOQUINODIMETHANE

Due to the simplicity it would lend to the design of enzyme electrodes, there has been increasing attention paid to the direct electron transfer between an electrode and the active center of redox enzymes (109-115). Recently, several studies have appeared describing the response of glucose oxidase (a flavoenzyme) at various forms of solid carbon electrodes (113-115). These studies indicate that the observed response is a function of the type of carbon used as the electrode material. At glassy carbon electrodes, glucose oxidase showed no electroactivity in the presence of glucose in the potential window -0.3 to +0.5 V versus SCE (113). At a medium porosity spectroscopic grade graphite electrode (a more "active" surface), the electrochemistry of glucose oxidase proceeds irreversibly with an overvoltage of 0.8 V versus SCE (115). To date, no studies have been reported describing the response of flavoenzymes at an unmodified rough pyrolytic graphite electrode (RPGE) which is generally one of the most "active" carbon surfaces (116). Therefore, described in this chapter is the behavior of a xanthine oxidase immobilized enzyme electrode constructed with RPG as the electrode material. The response obtained at RPG will be compared to that obtained at a TTF-TCNQ electrode.

In addition to carbon electrodes, platinum, Pt, and other inert metals have been used as electrode materials in the construction of enzyme electrodes (109-112). The results of these studies highlight the importance of electrostatics at the electrode/enzyme interface. Several redox proteins (cytochromes, ferredoxins and copper "blue" proteins) were found to give irreversible or nonexistent voltammetric responses at noble metal electrodes. The electrochemistry of these proteins can, however, be promoted by electrode modification (109,112) or by multivalent cations (110,111) giving rise to quasi-reversible responses. The response of xanthine oxidase at a Pt electrode has not been previously reported. The behavior of a xanthine oxidase immobilized enzyme electrode using Pt as the electrode material is evaluated and will be discussed in this chapter.

Furthermore, this chapter describes the use of TTF-TCNQ as an electrode material in amperometric enzyme electrodes. The analytical response of the xanthine oxidase membrane electrode constructed using TTF-TCNQ to the biological purines: xanthine, hypoxanthine and purine, and the thiopurines: 6-MP and 6-TX is presented. The kinetics of the xanthine oxidase membrane electrode response are described. In addition the application of this electrode to the analysis of biological purines in blood plasma is discussed. The response of an oxalate oxidase enzyme electrode with TTF-TCNQ as the electrode material to oxalate is also discussed.

3.1 Xanthine Oxidase Membrane Electrode with Rough Pyrolytic Graphite and Platinum as the Electrode Materials

Figure 3-1 illustrates schematically the design of the xanthine oxidase membrane electrode used in this investigation. With xanthine as the analyte, xanthine oxidase catalyzes the reaction scheme shown in equations 3.1 and 3.2:

$$\text{xanthine} + \text{xanthine oxidase/FAD} \longrightarrow \text{uric acid} + \text{xanthine oxidase/FADH}_2 \qquad \text{eq. 3.1}$$

$$\text{xanthine oxidase/FADH}_2 \longrightarrow \text{xanthine oxidase/FAD} + 2H^+ + 2e^- \qquad \text{eq. 3.2}$$

Under anaerobic conditions, reaction 3.2 occurs at the electrode surface. Figure 3-2A shows the response of a xanthine oxidase membrane electrode in a supporting electrolyte blank with RPG as the electrode material. The nature of the peaks at +0.58 V and -0.46 V are unknown. Following a 30-s incubation at an open circuit in a xanthine solution, an oxidation peak is observed at 0.4 V versus SCE on the initial sweep to positive potentials, Figure 3-2B. This oxidation peak occurs 0.5 V positive of the formal potential, $E^{0'}$, of xanthine oxidase (117) and 0.23 V negative of the E_{Pa} of the oxidation peak of xanthine at a bare RPCE (118). This oxidation peak occurs 0.3 V negative of that reported at a medium porosity spectroscopic grade graphite electrode (113).

As shown in equation 3.1, uric acid is the product of the xanthine-xanthine oxidase enzymatic reaction (28). Uric acid is electroactive and has been shown to undergo electrooxidation at RPGE

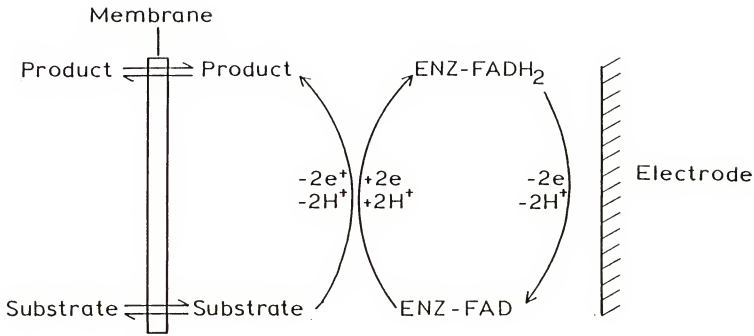

Figure 3-1. Schematic diagram of the flavoenzyme-membrane electrode.

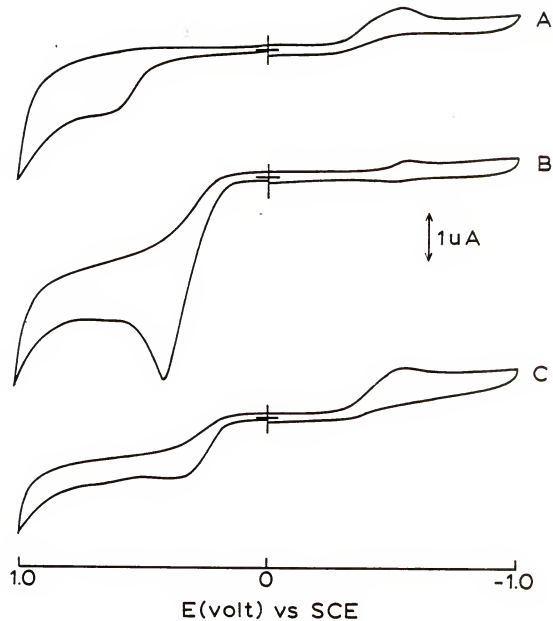

Figure 3-2. Cyclic voltammograms of xanthine oxidase membrane in 0.5 M, pH 8.0 phosphate buffer, 0.050 mL of 90 μM xanthine oxidase trapped at electrode surface: (A) electrolyte blank; (B) 0.66 mM xanthine; (C) 0.62 mM uric acid. Scan rate = 5 mV s^{-1}, initial sweep to positive potentials, electrode material RPGE, electrode area = 0.020 cm^2.

at 0.23 V versus SCE (118). Therefore, to ascertain whether the observed response in Figure 3-2B is due to the electrooxidation of $FADH_2$ (equation 3.2) or due to uric acid oxidation, the response of the membrane electrode in a uric acid solution was evaluated, Figure 3-2C. In the presence of uric acid, the response of the membrane electrode is similar to that shown in Figure 3-2B. On scans to positive potentials, an oxidation peak is observed at 0.4 V. This suggests that uric acid is the electroactive species reacting at the electrode to yield the observed response. The difference between the current response of the membrane electrode in the uric acid and xanthine solutions may be accounted for by mass transfer resistance within the membrane. Recent studies showed that the calculated flux of ferrocyanide was decreased by a factor of 2000-8000 for transport through enzyme matrices (119). With xanthine as the analyte, the enzymatic reaction causes an accumulation of uric acid at the electrode surface. While with uric acid in solution, the amount of the electroactive species at the electrode surface is lower because of the resistance to mass transfer. These preliminary studies suggest that uric acid oxidation may be the process which gives rise to the oxidation peak at 0.4 V.

Uric acid is known to react at a RPGE in an adsorption-controlled process (118). In repetitive scan experiments, the electrode loses sensitivity. For that reason, RPG was not pursued as an electrode material in the design of the sensor shown in Figure 3-1.

Figure 3-3. Cyclic voltammograms in 0.5 M, pH 8.0 phosphate buffer: (A) 0.66 mM xanthine at bare Pt electrode, (B) supporting electrolyte blank at xanthine oxidase membrane electrode (0.050 mL of 90 μM xanthine oxidase trapped at electrode surface); (C) 0.66 mM xanthine at xanthine oxidase membrane electrode. Scan rate = 5 mV s^{-1}, initial scan to positive potentials, electrode area ca. 0.020 cm^2.

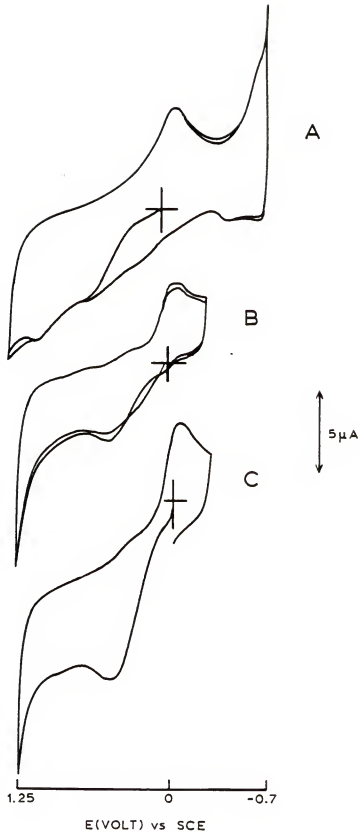
A
B
C
5μA
1.25
0
-0.7
E(VOLT) vs SCE

In order to evaluate the response of xanthine oxidase at a Pt electrode, the above experiments were repeated using Pt as the electrode material in the sensor design, Figure 3-1. Figure 3-3A shows the response of xanthine at a bare Pt electrode. On initial sweeps to positive potentials, a drawn out oxidation peak is observed at ca. 0.42 V versus SCE overlapping a Pt oxidation peak, and on repetitive scans the current diminishes in magnitude. Figure 3-3B shows a cyclic voltammogram of the xanthine oxidase membrane electrode in a supporting electrolyte blank. On the initial sweep to positive potentials, a Pt oxidation peak is observed at ca. 0.39 V. Figure 3-3C shows the response of the membrane electrode in the presence of xanthine. On the scan to positive potentials, the oxidation peak at ca. 0.40 V increases. At the membrane electrode (Figure 3-3C), the xanthine oxidation peak occurs at the same potentials as at a bare Pt electrode (Figure 3-3A). It is clear from the results in Figure 3-3 that the reproducibility and sensitivity of the measurements at Pt is poor; therefore, the use of this material was not pursued as an electrode in the design of the sensor depicted in Figure 3-1.

3.2 Tetrathiafulvalene Tetracyanoquinodimethane Electrode Characterization

The behavior of the TTF-TCNQ electrode is dependent on the supporting electrolyte (49). As a means of insuring that the TTF-TCNQ salt was properly prepared, its response in different supporting electrolytes was evaluated, and the results obtained were compared to those reported in the literature (49). A slurry of

TTF-TCNQ and THF was prepared without PVC, and as the slurry consistency thickened it was pressed into the electrode cavity. Figure 3-4A shows the response of this electrode in 1.0 M potassium acetate. The electrode exhibits a stable potential window in the region between -0.2 and 0.4 V versus SCE. This behavior is in good agreement with what has been reported for this medium (49). However, the electrode lacked mechanical strength and the electrode salt separated from the electrode cavity. To alleviate this problem, an electrode was prepared with one part PVC to nine parts salt (w/w). Figure 3-4B shows the response of the TTF-TCNQ:PVC electrode in pH 7.0 phosphate buffer. On the initial sweep to positive potentials, an oxidation peak is observed at +0.275 V, and a cathodic peak is observed at +0.009 V on the subsequent sweep to negative potentials. This electrochemical behavior is consistent with that for TTF-TCNQ in chloride-containing supporting electrolytes (49). The anodic peak has been attributed to the formation of $TTF^{+}Cl^{-}_{(s)}$ described by equation 3.3.

$$TTF^{o}_{(s)} - e^{-} + Cl^{-}_{(aq)} \longrightarrow TTF^{+}Cl^{-}_{(s)} \qquad \text{eq. 3.3}$$

while the cathodic peak represents the reduction of $TTF^{+}Cl^{-}_{(s)}$ in the reverse of equation 3.3 (49). It was, therefore, concluded that $TTF^{+}Cl^{-}_{(s)}$ was formed in the oxidation of the TTF-TCNQ:PVC electrode giving rise to the electrochemical behavior observed in a chloride-free supporting electrolyte. Chloride was likely an impurity in the

Figure 3-4. Cyclic voltammograms of TTF-TCNQ electrodes prepared: (A) 1:1 TTF-TCNQ (w/w) without PVC in 1.0 M potassium acetate; (B) 9:1 TTF-TCNQ to PVC (w/w) in 0.5 M, pH 7.0 phosphate buffer, (C) 9:1 TTF-TCNQ to PVC (w/w) in 0.5 M, pH 7.0 phosphate buffer and 0.15 M NaCl. Scan rate = 5 mV s^{-1}, initial sweeps to positive potentials, electrode area = 0.10 cm^2.

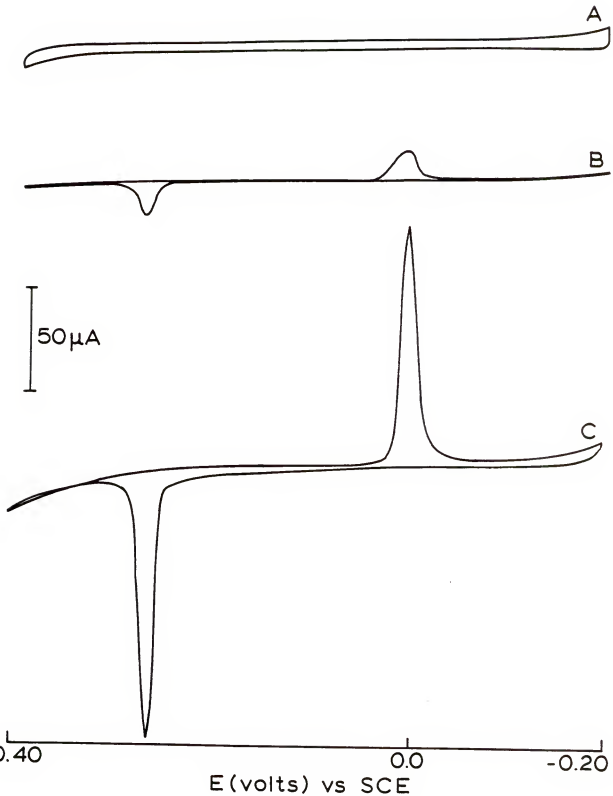
A
B
50μA
C
0.40
0.0
-0.20
E (volts) vs SCE

PVC. Figure 3-4C shows the response of the electrode in a 0.15 M sodium chloride-containing supporting electrolyte. It is clear from a comparison of the cyclic voltammogram in Figures 3-4B and 3-4C that the anodic and cathodic peaks observed in the chloride-free supporting electrolyte occur at potentials of the formation and reduction of $TTF^{+}Cl^{-}_{(s)}$. It was found in later experiments that by dissolving the PVC twice in THF and by reducing its concentration in the slurry the chloride impurity could be eliminated. These experiments confirmed that the polymer-paste electrode showed behavior in good agreement with that previously reported for high pressure pressed TTF-TCNQ electrodes in the absence of PVC.

According to recent reports, the $FADH_2$ redox center of the flavoenzyme glucose oxidase can be electrooxidized at a TTF-TCNQ electrode (21-23). However, no results were presented to illustrate the analytical response of the enzyme at this electrode surface. The membrane electrode construction design was optimized using glucose oxidase as the immobilized enzyme. As shown in Figure 3-5B, in the presence of glucose the current at the bare TTF-TCNQ electrode does not increase above the background current. In the same potential window, the enzyme of the membrane electrode exhibits a small increase in current. In the presence of glucose, a drawn out current response, Figure 3-5D, is observed which shows a significant increase over background at potentials from ca. +0.2 to 0.225 V versus SCE where $FADH_2$ has been reported to react at this electrode (23). Current readings were made at +0.225 V where the signal to noise

Figure 3-5. Cyclic voltammograms in 0.5 M, pH 7.0 phosphate buffer at bare TTF-TCNQ electrode in the (A) absence and (B) presence of 10 mM glucose, and at a glucose oxidase membrane electrode in the (C) absence and (D) presence of 10 mM glucose. Scan rate = 5 mV s^{-1}, initial sweeps to positive potentials, 0.050 mL of 0.1 mM glucose oxidase solution trapped at electrode surface.

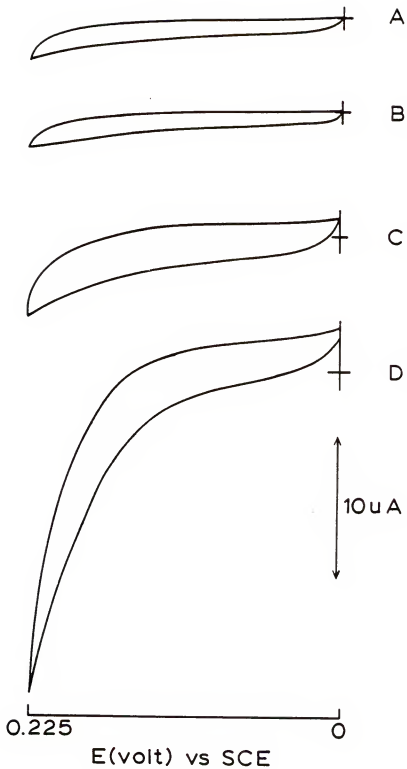
A
B
C
D
10uA
0.225
0
E(volt) vs SCE

ratio is the greatest (e.g., for a 10 mM glucose solution the signal to noise ratio is 5.5:1).

For an amperometric enzyme membrane electrode, when the diffusion layer is much greater than the reaction layer and the enzyme is unsaturated, equation 3.4 shows the current dependence on the substrate concentration (120):

$$i = nAF(Dk_{cat}[S]/K_M)^{1/2}e_\Sigma \qquad \text{eq. 3.4}$$

When the enzyme is saturated, equation 3.5 applies (120):

$$i = nAF(Dk_{cat})^{1/2}e_\Sigma \qquad \text{eq. 3.5}$$

where n is the number of electrons per mole of oxidized species, A is the electrode area (cm^2), F is Faraday's constant (96,486 coulombs per equivalent), D is the diffusion coefficient ($cm^2\ s^{-1}$), K_M is the Michaelis-Menten constant ($M\ cm^{-3}$), k_{cat} is the catalytic rate constant for the enzymatic reaction (units depend on the reaction order) and e_Σ is the total enzyme concentration ($M\ cm^{-3}$) (120). Under saturated conditions, the response of the membrane electrode becomes independent of substrate concentration, equation 3.5.

Figure 3-6 shows the steady-state calibration curve at the glucose oxidase membrane electrode obtained for glucose in pH 7.0 phosphate buffer. The response of the membrane electrode is linear in the concentration range from 1×10^{-3} to 1×10^{-2} M. The change in the slope of the current versus concentration plot is indicative of enzyme saturation kinetics where the reaction rate between the

Figure 3-6. Calibration curve for glucose at glucose oxidase membrane electrode in 0.5 M, pH 7.0 phosphate buffer. Steady-state response measured at +0.225 V versus SCE. Electrode material TTF-TCNQ.

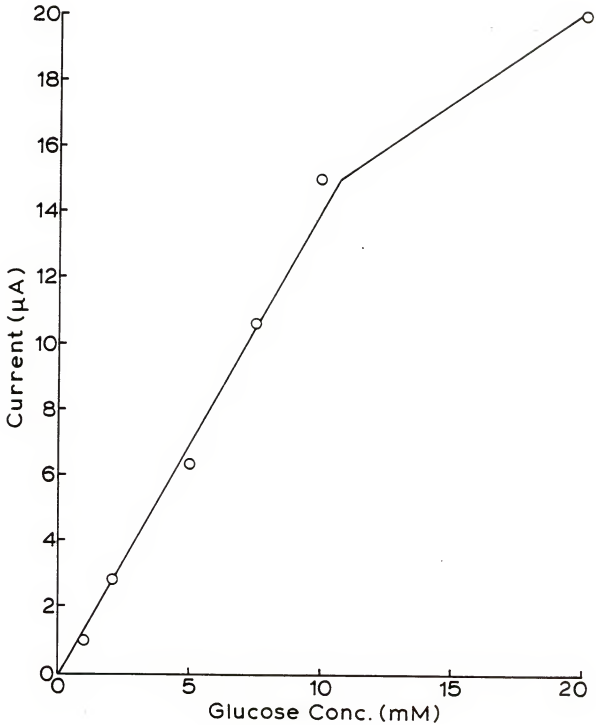
20
18
16
14
12
10
8
6
4
2
0
Current (μA)
0
5
10
15
20
Glucose Conc. (mM)

enzyme and substrate (as measured by current) becomes independent of substrate concentration. The linear dynamic range and the sensitivity at the glucose oxidase membrane electrode are in good agreement with that reported in the literature (23).

3.3 Xanthine Oxidase Membrane Electrode with Tetrathiafulvalene Tetracyanoquinodimethane as Electrode Materials

3.3.1 Analytical Response to Purines in Phosphate Buffer

With purine as the analyte, two reactions determine the response of the electrode:

$$\text{purine} + \text{xanthine oxidase/FAD} \longrightarrow \text{uric acid} + \text{xanthine oxidase/FADH}_2 \qquad \text{eq. 3.6}$$

$$\text{xanthine oxidase/FADH}_2 \longrightarrow \text{xanthine oxidase/FAD} + 2H^+ + 2e^- \qquad \text{eq. 3.7}$$

where under anaerobic conditions, reaction 3.7 occurs at the electrode surface. Cyclic voltammetry of the xanthine oxidase substrates hypoxanthine, xanthine, purine, 6-MP and 6-TX were performed at a bare and enzyme covered TTF-TCNQ electrode. Figure 3-7 shows the response of purine at a bare TTF-TCNQ electrode and at the membrane electrode illustrated schematically in Figure 3-1. As shown in Figure 3-7A, in the presence of purine the current at the bare TTF-TCNQ electrode does not increase above the background current. In the same potential window, the enzyme of the membrane electrode is not electroactive in the absence of substrate, and the response is the same as that in Figure 3-7A. In the presence of purine, Figure 3-7B, a drawn out cyclic voltammogram peak is observed

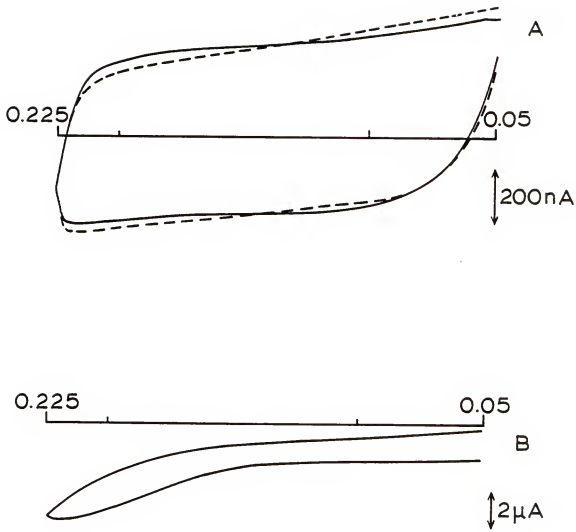

Figure 3-7. Cyclic voltammograms in 0.5 M, pH 8.0 phosphate buffer: (A) TTF-TCNQ electrode in the absence (----) and in the presence (——) of 0.455 mM purine (the response of the xanthine oxidase membrane electrode in the absence of purine is the same as (----)); (B) xanthine oxidase membrane electrode in 0.455 mM purine solution. Scan rate = 5 mV s^{-1}, initial sweep to positive potentials, 0.050 mL of 90 μM xanthine oxidase solution trapped at electrode surface.

which shows a significant current increase over background at ca. 0.2 V. This behavior is similar to that seen for the glucose oxidase membrane electrode in the presence of glucose, Figure 3-5D. The highest current signal to noise ratio is at potentials of 0.225 V (e.g., for 0.4 mM substrate concentrations, signal to noise ratios of ca. 150:1 are observed).

The current values measured at 0.225 V at bare and enzyme covered TTF-TCNQ electrodes in 4×10^{-4} M solutions of the five substrates of xanthine oxidase are summarized in Table 3-1. As shown in Table 3-1, purine shows the greatest current increase at the membrane electrode followed by xanthine and hypoxanthine. It is also clear from Table 3-1 that 6-TX and 6-MP show electroactivity at 0.225 V at the bare TTF-TCNQ electrode. For 6-TX and 6-MP, a current decrease is noted at the membrane electrode in the presence of enzyme, Table 3-1. The lower sensitivity of the enzyme electrode to the thiopurines is probably due in part to the fact that the endproduct of the thiopurine-xanthine oxidase enzymatic reaction is 6-thiouric acid (26). 6-Thiouric acid is an inhibitor of xanthine oxidase (121).

The analytical response of the xanthine oxidase membrane electrode to purine, hypoxanthine and xanthine was investigated. To shorten the analysis time, analytical results were obtained using constant potential measurements. In these measurements, the potential of the membrane electrode was poised at +0.225 V versus SCE, and the current measured after steady-state was reached (30-60 s).

Table 3-1. Comparison of Bare and Membrane Electrode Response

substrate[a]	x 10^{-4} M	bare[b] electrode current, μA	membrane[c] electrode current, μA
purine	4.55	0.009 ± 0.004	1.74 ± 0.01
hypoxanthine	4.54	0.008 ± 0.002	0.84 ± 0.02
xanthine	4.78	0.010 ± 0.003	0.95 ± 0.06
6-thioxanthine	4.32	0.485 ± 0.052	0.36 ± 0.01
6-mercaptopurine	4.24	1.127 ± 0.181	0.72 ± 0.01

[a] 0.5 M phosphate buffer, pH 8.0 at 225 mV versus SCE from cyclic voltammetry.

[b] TTF-TCNQ electrode.

[c] TTF-TCNQ electrode on which xanthine oxidase is immobilized with a porous dialysis membrane, MW cutoff: 6000-8000.

To evaluate the analytical potential of the xanthine oxidase membrane electrode, calibration curves for the three substrates (purine, hypoxanthine and xanthine) that exhibit current enhancement in the presence of the enzyme were obtained in deaerated solutions.

Figure 3-8 shows steady-state calibration curves obtained in 0.5 M, pH 8.0 phosphate buffer at the xanthine oxidase membrane electrode. In the linear portion of the calibration curves, the electrode response is rapid, reaching steady-state in 30-60 s. The analytical figures of merit for the three substrates are summarized in Table 3-2. As shown in Figure 3-8 and Table 3-2, the highest sensitivity (the greatest slope) is obtained for purine in agreement with the results in Table 3-1. The reason for this behavior is apparent from equation 3-8.

$$\text{purine} \xrightarrow[\text{oxidase}]{\text{xanthine}} \text{hypoxanthine} \xrightarrow[\text{oxidase}]{\text{xanthine}}$$

$$\text{xanthine} \xrightarrow[\text{oxidase}]{\text{xanthine}} \text{uric acid} \qquad \text{eq. 3.8}$$

As shown in equation 3.8, purine acts as a substrate of xanthine oxidase forming hypoxanthine; hypoxanthine is then converted by the enzyme to xanthine which also acts as a substrate of xanthine oxidase, and is converted to the final endproduct uric acid (28). In this reaction, the purine substrate effectively turns over three times. In agreement with equation 3.8, hypoxanthine shows intermediate sensitivity by effectively turning over twice, and the lowest sensitivity is observed for xanthine which only turns over

Figure 3-8. Calibration curves for purine, xanthine and hypoxanthine in 0.5 M, pH 8.0 phosphate buffer. Steady-state current measured at +0.225 V versus SCE.

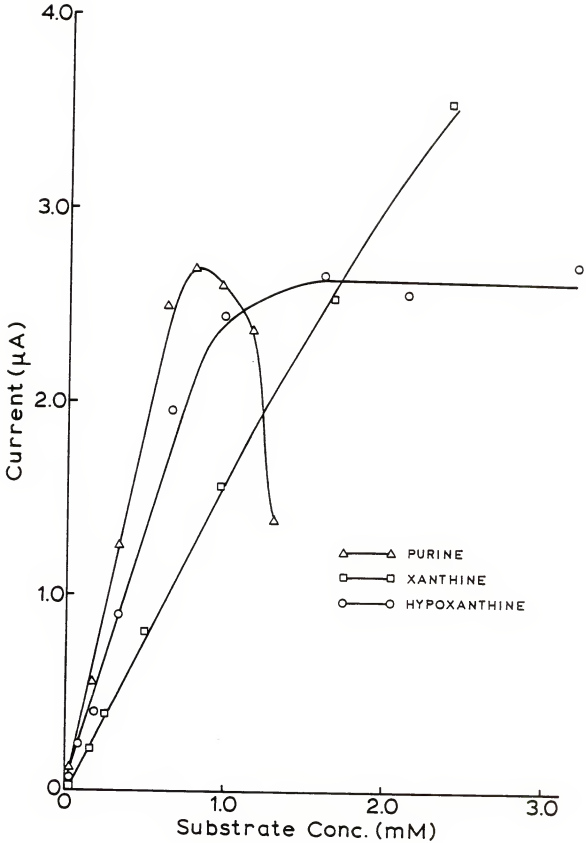
4.0
3.0
2.0
1.0
0
Current (μA)
0
1.0
2.0
3.0
Substrate Conc. (mM)
PURINE
XANTHINE
HYPOXANTHINE

Table 3-2. Xanthine Oxidase Membrane Electrode Response in Phosphate Buffer

substrate[a]	linear range[b], M	slope, $\mu A\ mM^{-1}$	intercept, μA	corr. coeff.
purine	$1.6 \times 10^{-5} - 6.4 \times 10^{-4}$	3.96±0.11	-0.022±0.042	0.9992
hypoxanthine	$1.6 \times 10^{-5} - 6.4 \times 10^{-4}$	3.12±0.08	-0.052±0.027	0.9989
xanthine	$1.2 \times 10^{-5} - 1.7 \times 10^{-3}$	1.51±0.03	0.054±0.027	0.9986

[a] All solutions prepared in 0.5 M, pH 8.0 phosphate buffer.

[b] TTF-TCNQ electrode on which xanthine oxidase is immobilized with a porous dialysis membrane; MW cutoff 6000-8000.

once (Figure 3-8 and Table 3-2). As shown in Figure 3-8, at concentrations above 1.7 mM xanthine, 0.63 mM hypoxanthine and 0.63 mM purine, the current response is no longer linear.

The shape of the current versus concentration plot for hypoxanthine (Figure 3-8) is characteristic of saturated enzyme kinetics where the reaction rate between the enzyme and the substrate (as measured by current) becomes independent of substrate concentration (87, p. 64). As shown in Figure 3-8, this limit is not reached for xanthine in the same concentration range. Higher xanthine concentrations were not tested due to the poor solubility of xanthine in phosphate buffer. The behavior observed for purine, where a decrease in current response is observed at high concentrations, is typical of autoinhibition effects known to occur in reactions catalyzed by xanthine oxidase (26).

3.3.2 Analysis of Purine and Hypoxanthine in Blood Plasma

The response of the membrane electrode to purine substrates in blood plasma was evaluated. Due to its poor solubility in blood plasma xanthine was not analyzed. Figure 3-9 shows the steady-state response of the membrane electrode to hypoxanthine and purine. The background current obtained in a plasma blank was subtracted from the data shown in Figure 3-9. The analytical figures of merit are summarized in Table 3-3. In comparison to the response observed in phosphate buffer (Table 3-2), the plasma matrix causes a decrease in sensitivity and linear dynamic range of the membrane electrode. Nevertheless, the electrode can easily be applied to analysis in a plasma matrix.

Figure 3-9. Calibration curves for purine and hypoxanthine at a xanthine oxidase membrane electrode in pH 7.7 blood plasma. Steady-state response measured at +0.225 V versus SCE.

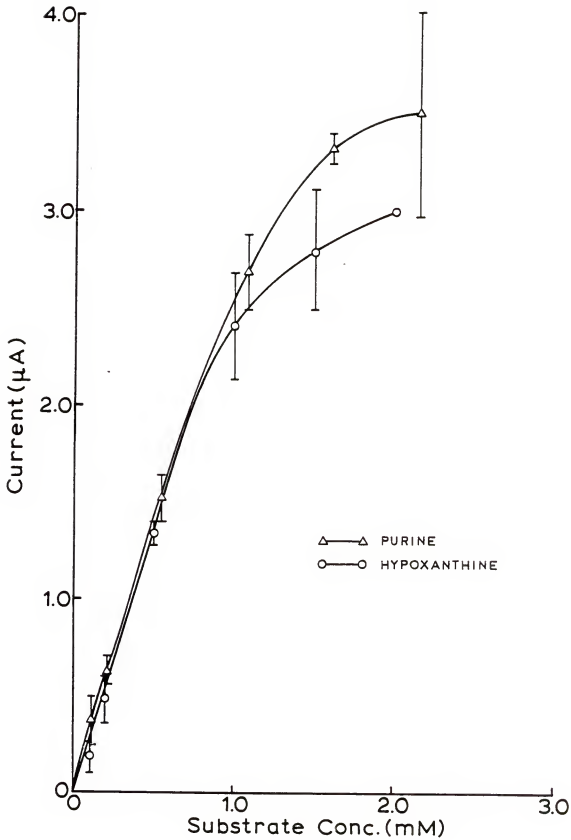
4.0
3.0
2.0
1.0
0
Current (μA)
0
1.0
2.0
3.0
Substrate Conc. (mM)
PURINE
HYPOXANTHINE

Table 3-3. Xanthine Oxidase Membrane Electrode Response in Blood Plasma

substrate[a]	linear range[b], M	slope, $\mu A\ mM^{-1}$	intercept, μA	corr. coeff.
hypoxanthine	$1.0 \times 10^{-4} - 1.0 \times 10^{-3}$	2.45±0.13	-0.007±0.007	0.9973
xanthine	$1.1 \times 10^{-4} - 1.1 \times 10^{-3}$	2.44±0.10	0.13 ±0.06	0.9983

[a] All solutions prepared in pH 7.7 blood plasma.

[b] TTF-TCNQ electrode on which xanthine oxidase is immobilized with a porous dialysis membrane. Steady-state response measured at +225 mV versus SCE.

3.3.3 Uric Acid Interference Study

Uric acid is a known competitive inhibitor of xanthine oxidase and binds reversibly to the enzyme (121). As a result, the substrate is denied access to the enzyme active site, and in homogeneous solution there is a decrease in the observed reaction rate in the presence of uric acid (32, p. 245). The dissociation constant for the enzyme-inhibitor complex in homogeneous solution is defined by equation 3.9.

$$K_i = \frac{[E][I]}{[EI]} \qquad \text{eq. 3.9}$$

where K_i has a value of 1.4×10^{-4} M for the xanthine oxidase-uric acid complex in homogeneous solution (121).

According to equation 3.8 each purine substrate reacts with xanthine oxidase to form uric acid as the final product. Therefore, the effect of uric acid on the response of the xanthine oxidase membrane electrode was evaluated by comparing the response to xanthine in the presence and absence of 4.8×10^{-4} M uric acid. This uric acid concentration is the upper normal blood level in healthy males and represents the highest uric acid concentration in a normal population (2, pp. 264-268).

Assuming the concentration of the xanthine oxidase-uric acid complex is insignificant relative to the uric acid concentration, equation 3.9 indicates that two-thirds of the enzyme is bound and inaccessible to the substrate. Therefore, in the presence of the above uric acid concentration, a decrease in the membrane electrode

sensitivity is anticipated. Figure 3-10 shows the current versus xanthine concentration plots in the presence and absence of uric acid. It is clear from Figure 3-10 that the slopes of the two plots are essentially the same, Table 3-4. The calibration curve obtained in the presence of uric acid has a higher intercept, Table 3-4. Contrary to what is observed in homogeneous solution, uric acid is not inhibiting the xanthine oxidase of the membrane electrode. The increase in the membrane electrode response (increased intercept) is probably the result of the direct electrooxidation of uric acid at the TTF-TCNQ electrode.

Figure 3-11 shows the current versus uric acid concentration calibration curve at a bare TTF-TCNQ electrode. The sensitivity shown in Figure 3-11 is lower than that observed for xanthine at a xanthine oxidase membrane electrode, Table 3-4. Figure 3-11 also shows the response of uric acid at a xanthine oxidase membrane electrode. As expected, this response is lower than that observed at a bare electrode. The sensitivity is three times lower than that obtained for xanthine at the membrane electrode, Table 3-4. Based on these results it is apparent that, although uric acid does react at the TTF-TCNQ electrode, the $FADH_2$ redox center of xanthine oxidase must contribute to the analytical signal. Further evidence that $FADH_2$ oxidation occurs at the electrode surface is obtained from the examination of equation 3.8. As illustrated in this reaction, each substrate reacts with xanthine oxidase to form uric acid as the endproduct. If the analytical signal was due solely to uric acid

Figure 3-10. Calibration curves for xanthine at xanthine oxidase membrane electrode in 0.5 M, pH 8.0 phosphate buffer. In the absence (●——●) and in the presence of (O——O) of 0.48 mM uric acid. Steady-state response measured at +0.225 V versus SCE.

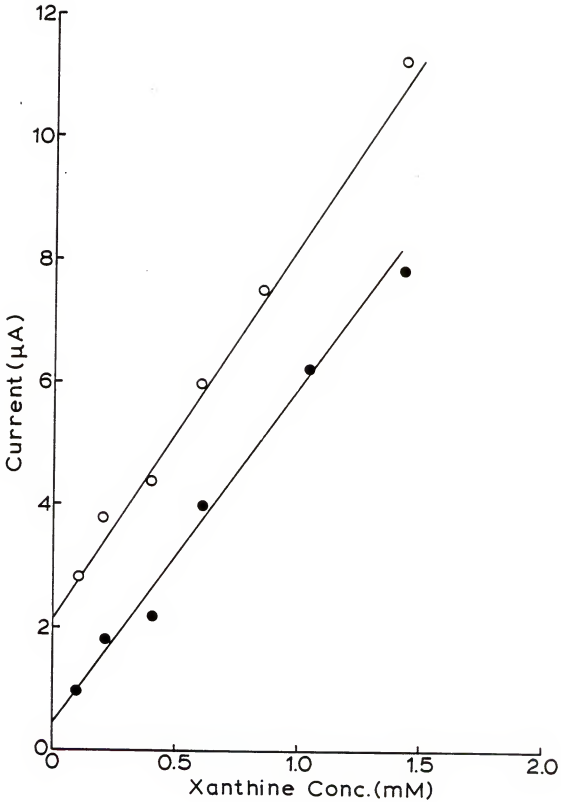
12
10
8
6
4
2
0
Current (μA)
0
0.5
1.0
1.5
2.0
Xanthine Conc.(mM)

Table 3-4. Uric Acid Interference Study

compound[a]	slope, μA mM^{-1}	intercept, μA	corr. coeff.
xanthine[b]	5.61	0.51	0.9938
xanthine + 0.48 mM uric acid[b]	5.93	2.24	0.9975
uric acid[b]	1.87	0.10	0.9989
uric acid[c]	3.96	0.18	0.9986

[a] All solutions prepared in 0.5 M, pH 8.0 phosphate buffer. Current measured at 225 mV versus SCE from cyclic voltammetry.

[b] TTF-TCNQ electrode on which xanthine oxidase is immobilized with a porous dialysis membrane; MW cutoff: 6000-8000.

[c] Bare TTF-TCNQ electrode.

Figure 3-11. Calibration curves or uric acid at a bare TTF-TCNQ electrode (O——O) and a xanthine oxidase membrane electrode (●——●). Steady-state response measured at +0.225 V versus SCE.

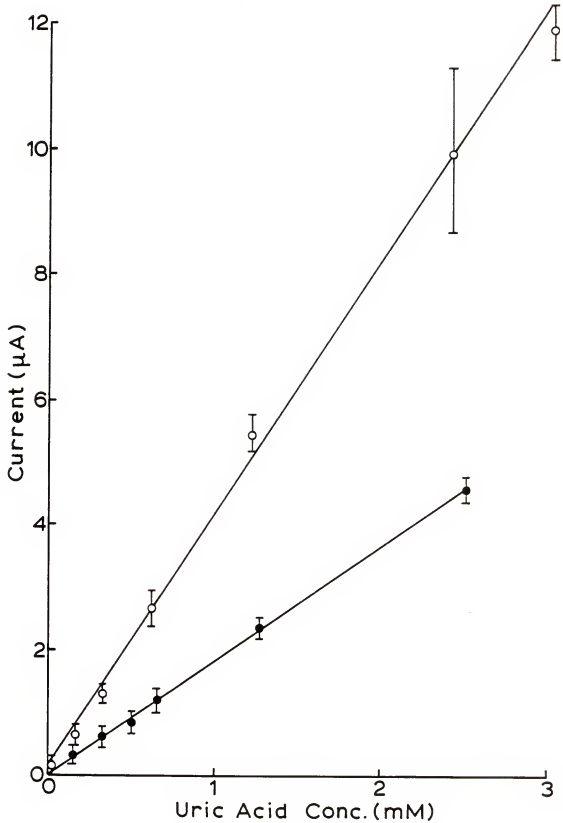
12
10
8
6
4
2
0
Current (μA)
0
1
2
3
Uric Acid Conc. (mM)

oxidation, than each substrate would show the same (or very similar) sensitivity at the membrane electrode. As shown in Figure 3-8 and Table 3-2, this is clearly not the case indicating that the $FADH_2$ redox center of xanthine oxidase must also be oxidized at the TTF-TCNQ electrode giving rise to the analytical signal.

3.3.4 Effect of Experimental Parameters on the Electrode Response

Enzymatic reactions are affected by solution pH and temperature and for flavoenzymes by oxygen concentration. The effects of these parameters on the response of the xanthine oxidase membrane electrode were, therefore, investigated.

The catalytic activity of xanthine oxidase in homogeneous solution increases with pH exhibiting a maximum activity at pH 8.0 (26). For homogeneous reactions, the shape of the pH-activity profile is a function of substrate concentration. The profiles are typically reported for concentrations at which the enzyme is saturated with substrate (59, p. 195, 122). At a purine concentration of 5×10^{-4} M, a concentration of substrate that saturates the enzyme in homogeneous reactions (26,122), the maximum response is observed at pH 6.5, Figure 3-12. In this study, in accordance with general practice the solution is maintained at the value reported to be optimum for xanthine oxidase (pH 8.0) on the basis of the reported pH-activity profiles (26,122).

Figure 3-13 shows the response of the membrane electrode to xanthine in nitrogen and oxygen-saturated phosphate buffers. Since oxygen is the ultimate electron acceptor for the $FADH_2$ redox center

Figure 3-12. Current response of xanthine oxidase membrane electrode at different pH values. The phosphate buffer was adjusted to the appropriate pH just prior to analysis. Purine concentration = 0.5 mM. Steady-state response measured at +0.225 V versus SCE.

Current (μA)
2.0
1.0
0
5.5
6.0
6.5
7.0
7.5
8.0
8.5
9.0
9.5
10.0
pH

Figure 3-13. Calibration curve for xanthine oxidase membrane electrode in oxygen and nitrogen-saturated 0.5 M, pH 8.0 phosphate buffer. Steady-state response measured at +0.225 V versus SCE.

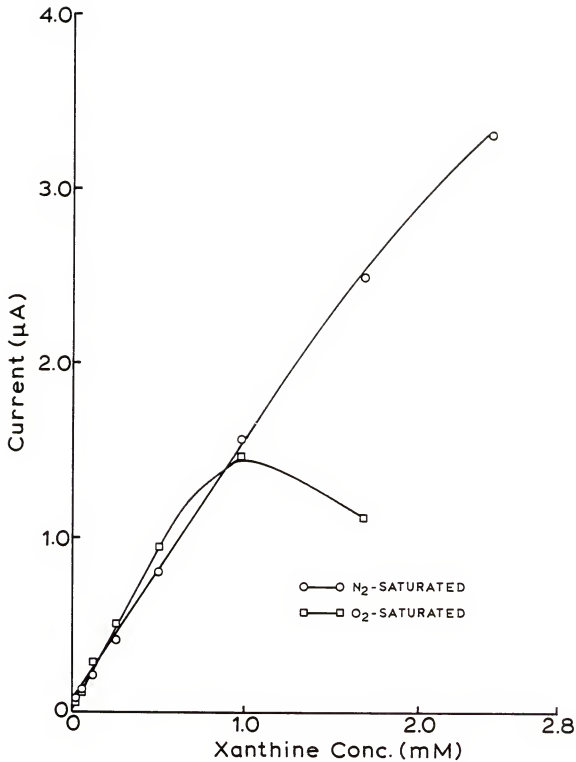
4.0
3.0
2.0
1.0
0
Current (μA)
0
1.0
2.0
2.8
Xanthine Conc. (mM)
N2-SATURATED
O2-SATURATED

of xanthine oxidase (28, p. 318, 87, p. 330), some interference from oxygen was anticipated. However, at xanthine concentrations less than 1.0 mM, oxygen did not interfere with the electrode response. The behavior illustrated in Figure 3-13 is reminiscent of enzyme saturation kinetics with oxygen interference becoming apparent only at high substrate concentrations. This probably reflects a lower concentration of $FADH_2$ groups that can be oxidized electrochemically in the presence of oxygen. Interference from oxygen only occurs at high substrate concentration and may indicate that the $FADH_2$ groups are not uniformly accessible to oxygen.

The response of the xanthine oxidase electrode is a function of temperature, Figure 3-14. As expected (94), the response decreases with decreasing temperature. A change in the slope of the Arrhenius-Van Hoff plot was observed at ca. 35°C which is in good agreement with that previously reported for immobilized xanthine oxidase and may be due to a change in enzyme conformation (18). That this process is reversible was established by obtaining the same response at 27°C before and after measurements at the highest temperature (45°C).

3.3.5 Stability of Xanthine Oxidase Membrane Electrode

Figure 3-15 shows the response of a single xanthine oxidase membrane electrode over a 48-hour period. The membrane electrode was stored in 0.5 M, pH 8.0 phosphate buffer at 4°C. The membrane electrode shows a 4% decrease in response to purine in 0.5 M, pH 8.0 phosphate buffer within 24 hours and a 63% decrease after 48 hours. As shown in Figure 3-15, the reproducibility of the response

Figure 3-14. Arrhenius-Van't Hoff plot for xanthine oxidase membrane electrode, purine concentration = 0.5 mM. Steady-state response measured at +0.225 V versus SCE.

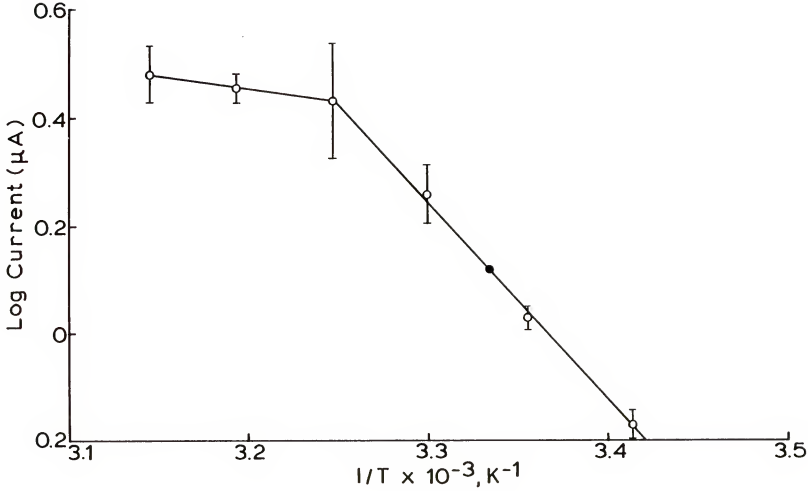
0.6
0.4
0.2
0
0.2
Log Current (μA)
3.1
3.2
3.3
3.4
3.5
1/T x 10⁻³, K⁻¹

Figure 3-15. Stability of xanthine oxidase membrane electrode, xanthine concentration = 0.5 mM. Steady-state measured at +0.225 V versus SCE. Membrane electrode stored in 0.5 M phosphate buffer at 4°C between measurements.

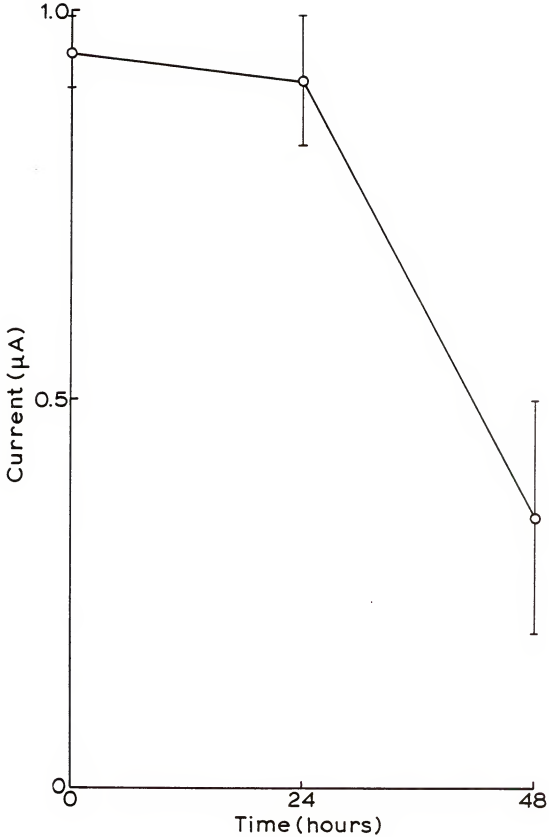
1.0
0.5
0
Current (μA)
0
24
48
Time (hours)

decreases with time. Xanthine oxidase has been shown to be particularly unstable in solution (18). The decrease in activity has been attributed to the dissociation of the flavin redox center from the enzyme (18). This could account for the observed decrease in response. Based on these results xanthine oxidase electrodes were prepared fresh daily.

3.3.6 Electrode Kinetics

The xanthine oxidase membrane electrode kinetics were analyzed using a recently developed theory (120) which assumes a model of enzyme kinetics illustrated in equation 3.10. According to this model, the enzyme (E) first combines with the substrate (S) to form an enzyme-substrate complex (ES) which reacts to form a new complex (E'P); in the last step this complex dissociates producing a new form of the enzyme (E'), e.g., reduced versus initial oxidized form (E), and the reaction product (P):

$$E + S \underset{k_{-1}}{\overset{k_1}{\rightleftharpoons}} ES \underset{k_{-2}}{\overset{k_2}{\rightleftharpoons}} E'P \underset{k_{-3}}{\overset{k_3}{\rightleftharpoons}} E' + P \qquad \text{eq. 3.10}$$

This model assumes steady-state Michaelis-Menten kinetics in which the concentration of the enzyme-substrate complex is small and constant. This assumption is valid provided that the total enzyme concentration, e_Σ, is small and constant (e.g., when $e_\Sigma \ll S$) (87, p. 64). The enzyme kinetics are then described by the Michaelis-Menten rate law, equation 3.11:

$$V = \frac{V_{max}[S]}{K_M + [S]} \qquad \text{eq. 3.11}$$

where K_M is the Michaelis-Menten constant which is that substrate concentration which gives half-maximal reaction velocity, V_{max}. The enzyme is half-saturated when $[S] = K_M$ (87, p. 64).

Under these conditions and in the absence of product inhibition, the following equation relates flux, j (mol cm^{-2} s^{-1}), at the membrane electrode to substrate concentration in solution, s_∞, and to the kinetics of the electrochemical and enzymatic reactions as well as to the membrane mass transport (120):

$$\frac{s_\infty}{j} = \frac{1}{k'_{ME}}\left[1 + \frac{s_\infty}{K_{ME}}\left(1 - \frac{j}{k'_s\, s_\infty}\right)\right] \qquad \text{eq. 3.12}$$

In equation 3.12, K_{ME} is the equivalent of the Michaelis-Menten constant. The system is unsaturated at substrate concentrations less than K_{ME} (120). The effective electrochemical rate constant, k'_{ME} (cm s^{-1}), is defined by equation 3.13:

$$\frac{1}{k'_{ME}} = \frac{K_M}{e_\Sigma\, L\, k_{cat}} + \frac{1}{k'_s} \qquad \text{eq. 3.13}$$

The value of k'_{ME} is determined by enzymatic kinetic parameters (first term of the right-hand side of equation 3-13) and by the kinetics of substrate mass transport through the membrane, where k'_s (cm s^{-1}) is the substrate mass transport rate constant. In equation 3.13, L is

the membrane thickness (cm) and K_M is the Michaelis-Menten constant for the homogeneous enzymatic reaction. The combined rate constant, k_{cat}, for the last two steps in the enzymatic reaction shown in equation 3.10 is given by equation 3.14:

$$k_{cat} = K_2 + \frac{k_2 k_3}{k_{-2}} + K_3 \qquad \text{eq. 3.14}$$

According to equation 3.12, in agreement with simple Michaelis-Menten kinetics, equation 3.10 (123, pp. 518-521) at the limit of low substrate concentrations the plot of the inverse of the electrochemical reaction rate (as measured by current, C s^{-1} cm^{-2}) normalized for substrate concentration (M cm^{-3}), nFA/i, versus substrate concentration has an intercept equal to the inverse of the effective electrochemical rate constant k'_{ME}. Such plots for the data shown in Figure 3-8 for the three substrates are shown in Figure 3-16. The values of k'_{ME}, obtained from the intercepts, are summarized in Table 3-5.

For values of s_∞/j significantly greater than $(s_\infty/j)_o$ a new variable, ρ, can be calculated where

$$\rho = (j/s_\infty)/(j/s_\infty)_o \leq 1 \qquad \text{eq. 3.15}$$

Since $(s_\infty/j)_o$ is equal to $(k'_{ME})^{-1}$ at the limit of $s \longrightarrow 0$, equation 3.15 reduces to

Figure 3-16. Normalized inverse flux (s_∞/j) versus substrate concentration, s_∞ (120) for data shown in Figure 3-8.

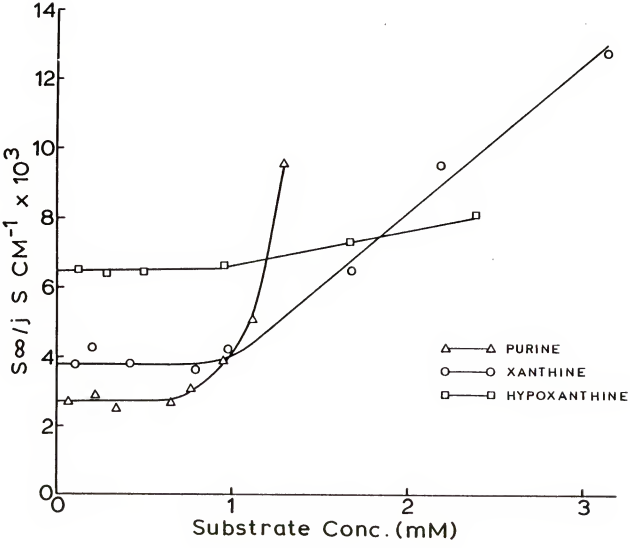
14
12
10
8
6
4
2
0
0
1
2
3
S∞/j S CM-1 x 10³
Substrate Conc. (mM)
PURINE
XANTHINE
HYPOXANTHINE

Table 3-5. Kinetic Results for Xanthine Oxidase Membrane Electrode in Phosphate Buffer

substrate[a]	k'_{ME},[b] cm s^{-1}	k'_S,[c] cm s^{-1}	ρ[c]	K_{ME},[c] M	V[d]	K_M,[e] M
xanthine	1.59×10^{-4}	1.59×10^{-4}	1.05	2.34×10^{-3}	2356	1.7×10^{-6}
hypoxanthine	2.60×10^{-4}	2.60×10^{-4}	1.01	9.67×10^{-4}	1336	1.3×10^{-6}
purine	3.62×10^{-4}	3.62×10^{-4}	0.981	6.18×10^{-4}	474	3×10^{-6}

[a] All solutions prepared in 0.5 M, pH 8.0 phosphate buffer.

[b] Obtained from Figure 3-16 plots (equation 3.12) of data shown in Figure 3-8.

[c] Obtained from Figure 3-17 plots (equation 3.17) of data shown in Figure 3-8.

[d] Obtained from Figure 3-18 slopes (equations 3.26 and 3.27) of data shown in Figure 3-8.

[e] References 26, 122.

$$\rho = \frac{i}{k'_{ME}[S]} \qquad \text{eq. 3.16}$$

where i is the current normalized for electrode area (C s^{-1} cm^{-2}) and [S] is substrate concentration (M cm^{-3}). Substitution in equation 3.17 gives

$$y = \frac{\rho^{-1} - 1}{s_\infty} = \frac{1}{K_{ME}} \left(1 - \frac{\rho\, k'_{ME}}{k'_s}\right) \qquad \text{eq. 3.17}$$

It is clear from equation 3.17 that a plot of y against ρ will allow the determination of K_{ME} from the intercept at $\rho = 0$, and from the intercept at $y = 0$ the ratio of k'_{ME}/k'_s. The plots of y versus ρ for the three substrates are shown in Figure 3-17 and the values of ρ at $y = 0$ (equation 3.17) are summarized in Table 3-5. As shown in Table 3-5, ρ values are ca. 1 when $y = 0$ for all three substrates. Therefore, in agreement with equation 3.17 the effective electrochemical rate constant values, k'_{ME}, are equal to the values of the mass transfer rate constants, k'_s, for all three substrates. These values are summarized in Table 3-5. According to equation 3.13 the equality of k'_{ME} and k'_s indicates that for this membrane electrode under conditions of unsaturated enzyme kinetics, i.e., in the linear portion of the current versus concentration curve, the rate of substrate mass transport through the membrane is the rate-limiting step. This is analytically the most desirable situation (23) since the enzymatic and electrochemical kinetics are fast by comparison and therefore do not affect the electrode response.

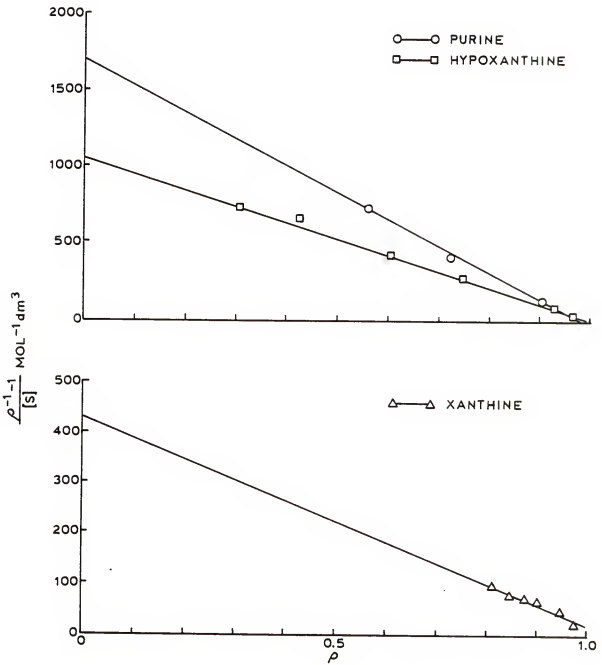

Figure 3-17. Plots of equation 3.17 (120) for data shown in Figure 3-8.

The mass transport rate constant k'_s is equivalent to membrane permeability, P_M (124,125). It has been shown that P_M values can be obtained from measurements using a rotating-disc electrode (RDE):

$$k'_s = P_M = \frac{\alpha D_M}{L} = \frac{D_{eff}}{L} \qquad \text{eq. 3.18}$$

where α is the substrate partition coefficient between the solution and the membrane and D_M ($cm^2\ s^{-1}$) is the substrate diffusion coefficient in the membrane (124). Values of k'_s (Table 3-5) obtained in this study are in good agreement with permeability values measured by RDE method for similar membranes and substrates (125).

From the values of the mass transport rate constants, k'_s, and the known membrane thickness L = 0.03 cm, an effective diffusion coefficient, D_{eff}, of the purine substrates through the membrane can be determined from equation 3.18. Our results indicate that at this membrane electrode for purine substrates $D_{eff} = 10^{-6}\ cm^2\ s^{-1}$.

The D_{eff} values obtained by the above treatment are in good agreement with those using equation 3.19 (126):

$$t_{ss} \leq \frac{1.5\ L^2}{D_M} \qquad \text{eq. 3.19}$$

In equation 3.19, t_{ss} is the time (s) at which the membrane electrode reaches steady-state and D_M equals D_{eff}. Using typical t_{ss} values of 45 s for the purine substrates at this membrane $D_{eff} = 10^{-6}\ cm^2\ s^{-1}$.

The observed increase in K_M values (Table 3-5) has been previously reported for immobilized enzyme electrodes (13,126). It

has also been predicted from a digital simulation of an immobilized enzyme electrode response under conditions of substrate diffusion (126). For these electrodes, the removal of the enzymatic reaction product in the electrode reaction gives rise to the analytical signal. This situation holds for the xanthine oxidase membrane electrode where the reduced flavin redox center and uric acid are oxidized at the TTF-TCNQ electrode (section 3.3.3). Therefore, the digital simulation model provides an additional means of evaluating the kinetic and diffusion properties of the membrane electrode.

In the simulation of the electrode response, the membrane of thickness d is divided into N equal volume elements. The width of each element Δx is given by equation 3.20.

$$\Delta x = \frac{d}{N} \qquad \text{eq. 3.20}$$

The assumption that the diffusion coefficient, D, is the same for both substrate and product leads to a known time parameter, d^2/D. Dividing this parameter by L equal intervals establishes t, the duration of a single iteration in the simulation, equation 3.21.

$$\Delta t = \frac{d^2}{DL} \qquad \text{eq. 3.21}$$

Diffusion can be simulated as the element-by-element transfer of matter between adjacent elements (104, pp. 416-428, 106, pp. 675-685).

Substrate, S, and product, P, concentrations are expressed relative to the bulk substrate concentrations, C. Fractional concentrations of the substrate, f_s, and product, f_p, are determined in each N volume element (numbered J, $1 \leq J \leq N$) during each iteration (numbered K, $K \geq 1$). In this manner, the concentration in the membrane can be determined using fractional concentrations, equation 3.22.

$$[S] = C \cdot f_s(J,K) \quad \text{and} \quad [P] = C \cdot f_p(J,K) \qquad \text{eq. 3.22}$$

Assuming the enzyme-kinetics illustrated in equation 3.10, the following equation relates product formation in the membrane to substrate concentration as well as enzymatic kinetics,

$$\frac{d[P]}{dt} = \frac{k_3 C_e}{(K_M/[S]) + 1} \qquad \text{eq. 3.23}$$

In finite difference representation, equation 3.23 becomes

$$C\Delta f_p(J,K) = \frac{k_3 C_e}{(K_M/C)/f_s(J,K) + 1} \qquad \text{eq. 3.24}$$

where C_e is the total enzyme concentration. Substitution of equation 3.21 into equation 3.24 and rearrangement yields equation 3.25 which is used to calculate the fractional change in product concentration in each volume element due to enzyme catalysis of the substrate contained in that volume element:

$$\Delta f_p(J,K) = \frac{(k_3 C_e d^2/DK_M)}{1 + (C/K_M) f_s(J,K)} \cdot \frac{f_s(J,K)}{L} \qquad \text{eq. 3.25}$$

Equation 3.25 contains two dimensionless parameters whose values can be varied in the simulation. One of the dimensionless parameters, C/K_M, compares the bulk substrate concentration with the Michaelis-Menten constant. Variation of this parameter shows the concentration dependence of the current. The other dimensionless variable is defined by the symbol V, equation 3.26:

$$V = \frac{k_3 C_e d^2}{DK_M} \qquad \text{eq. 3.26}$$

The variable V compares the rate of enzymatic reaction in the membrane to the rate of diffusion through the membrane. When V is greater than 10, the enzyme catalysis is rapid relative to substrate diffusion through the membrane.

Under conditions given in equation 3.10 and removal of enzymatic reaction product by the electrode reaction, digital simulation predicts the current response of an amperometric enzyme electrode in the limits of diffusion control will follow the relationship shown in equation 3.27.

$$\frac{nFAdk_3 C_e}{i_s} = \frac{k_3 C_e d^2}{DC} + 2 \qquad \text{eq. 3.27}$$

And the maximum steady-state current that can be achieved is

$$i_{max} = 1/2\ n\ FADK_3C_e \qquad \text{eq. 3.28}$$

In treating the xanthine oxidase membrane electrode experimental data, Figure 3-8, the ordinate was plotted as $i_s/2i_{max}$ which is equivalent to $i_s/nFAdK_3C_e$ (equation 3.27) and the abscissa was plotted as C/K_M (equations 3.26 and 3.27). For all three substrates, the concentrations were normalized by the known K_M values reported for homogeneous solution, Table 3-5. The slopes of the plots shown in Figure 3-18 are summarized in Table 3-5. It is clear from equation 3.27 that the value of V is given by the inverse of the slope of these plots. As shown in Table 3-5, the values of V are greater than 10. It can, therefore, be concluded that the xanthine oxidase membrane electrode operates under diffusion control for all three substrates. This is in agreement with what is obtained using the theory of Albery and Bartlett (120). The values of V are in good agreement for what is seen in the relative increase in K_{ME} versus K_M. The greater the increase in K_{ME} relative to K_M; the larger the value of V, Table 3-5.

Another useful approach to the analysis of the enzyme kinetic data are Lineweaver-Burke plots (32, p. 242). In this graphical analysis, plots are obtained by taking the reciprocal of the Michaelis-Menten equation:

$$\frac{1}{v} = \frac{K_M + [S]}{V\ [S]} \qquad \text{eq. 3.29}$$

Figure 3-18. Dimensionless calibration curves (126) for data shown in Figure 3-8.

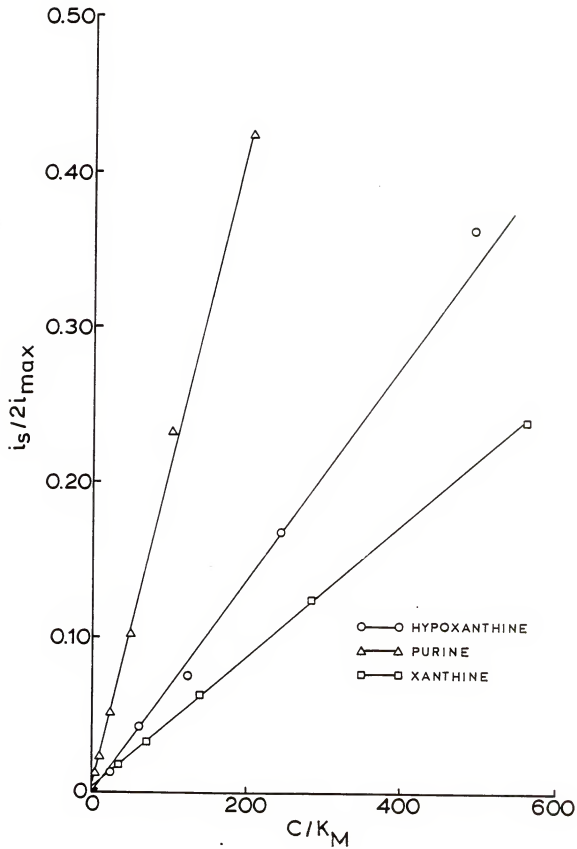
0.50
0.40
0.30
0.20
0.10
0
$i_s/2i_{max}$
0
200
400
600
C/K_M
HYPOXANTHINE
PURINE
XANTHINE

where v is the reaction rate (measured by current) and V is the maximum reaction rate. By rearranging equation 3.29, equation 3.30 is obtained.

$$\frac{1}{v} = \frac{1}{[S]} \frac{K_M}{V} + \frac{1}{V} \qquad \text{eq. 3.30}$$

which has the form y = mx + b. A graph of 1/v versus 1/[S] has a slope of K/V, a 1/v intercept of 1/V and a 1/[S] intercept of -1/K.

Double reciprocal plots of the current versus concentration for the three substrates were constructed and are shown in Figures 3-19 through 3-21. The solid lines connect the reciprocal maximum current, i_{max}, obtained experimentally and the reciprocal steady-state current for the lowest substrate concentration, Figure 3-8. Negative deviation from the typical Lineweaver-Burke behavior is observed in the case of each substrate. This type of deviation is predicted from the simulation model (126) when the enzyme kinetics are rapid relative to substrate mass transport through the membrane. However, other deviations of Michaelis-Menten kinetics can also cause the same type of Lineweaver-Burke plot shown in Figures 3-19 through 3-21 (e.g., product inhibition) (127, p. 130).

As in phosphate buffer, the electrode response in blood plasma is limited by the rate of mass transport through the membrane. This was verified by analysis of Figure 3-9 data using the methods described in this section. It was determined that the mass transfer rate constants k'_s for both substrates are lower in plasma than in phosphate buffer (Table 3-6). In practice, this means lower membrane

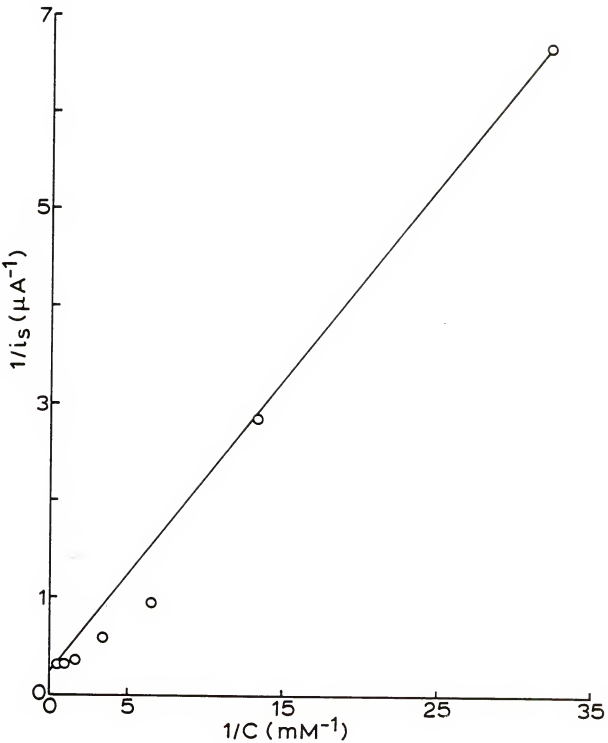

Figure 3-19. Lineweaver-Burke plot (32, p. 242) of the steady-state response of xanthine oxidase membrane electrode to purine for data shown in Figure 3-8.

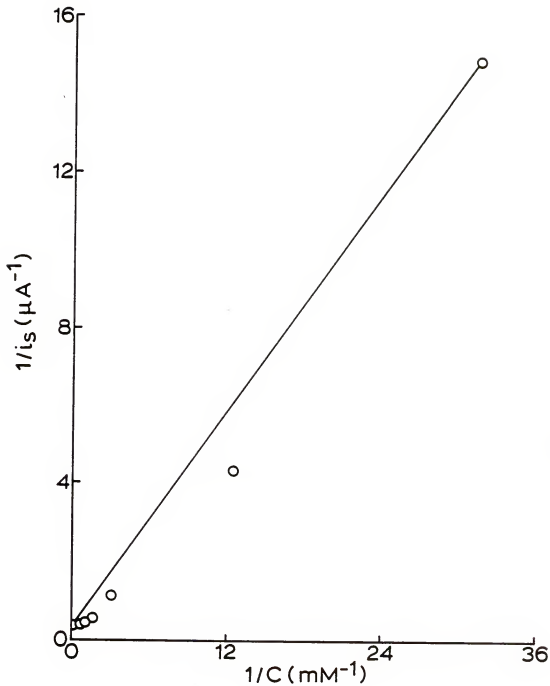

Figure 3-20. Lineweaver-Burke plot (32, p. 242) of the steady-state response of xanthine oxidase membrane electrode to hypoxanthine for data shown in Figure 3-8.

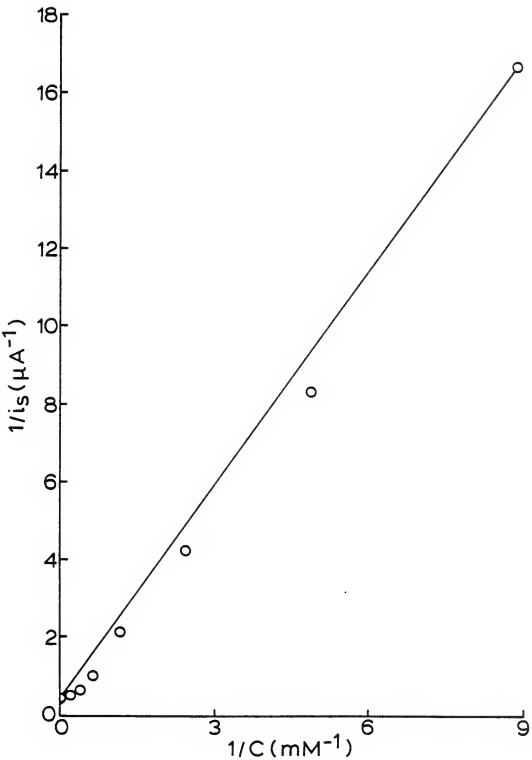

Figure 3-21. Lineweaver-Burke plot (32, p. 242) of the steady-state response of xanthine oxidase membrane electrode to xanthine for data shown in Figure 3-8

Table 3-6. Kinetic Results for Xanthine Oxidase Membrane Electrode in Blood Plasma

substrate[a]	k'_{ME},[b] cm s^{-1}	k'_S,[c] cm s^{-1}	ρ[c]	K_{ME},[c] M	V[d]	K_M,[e] M
hypoxanthine	2.32×10^{-4}	2.32×10^{-4}	1.01	1.27×10^{-3}	1279	1.3×10^{-6}
purine	2.85×10^{-4}	2.85×10^{-4}	1.10	1.30×10^{-3}	997	3×10^{-6}

[a] Solutions prepared in pH 7.7 blood plasma.

[b] Obtained from plots of equation 3.12 of data shown in Figure 3-9.

[c] Obtained from plots of y versus ρ according to equation 3.17 of data shown in Figure 3-9.

[d] Obtained from plots of equations 3.26 and 3.27 of data shown in Figure 3-9.

[e] References 26, 122.

permeability and lower effective diffusion coefficients probably caused by the interaction of large molecular weight components of plasma with the membrane.

3.4 Oxalate Oxidase Membrane Electrode with Tetrathiafulvalene Tetracyanoquinodimethane as Electrode Material

Unlike xanthine oxidase, oxalate oxidase is a flavoenzyme which reacts exclusively with molecular oxygen following the enzyme-analyte reaction in homogeneous solution (27,97,99). Therefore, oxalate oxidase served as a model in evaluating the acceptor capabilities of TTF-TCNQ with a flavoenzyme of high electron acceptor specificity.

The design of the oxalate oxidase membrane electrode was the same as that of xanthine oxidase, Figure 3-1. Under anaerobic conditions with oxalate as the analyte, the following reaction scheme occurs:

$$\text{oxalate} + \text{oxalate oxidase/FAD} \longrightarrow \text{oxalate oxidase/FADH}_2 + CO_2 + H_2O_2 \qquad \text{eq. 3.31}$$

$$\text{oxalate oxidase/FADH}_2 \longrightarrow \text{oxalate oxidase/FAD} + 2H^+ + 2e^- \qquad \text{eq. 3.32}$$

If TTF-TCNQ functions as an electron acceptor, reaction 3.32 should occur at the electrode surface giving rise to the analytical signal. Figure 3-22A shows the response of an oxalate oxidase membrane electrode in 0.05 M, pH 3.5 succinate buffer. As shown in Figure 3-22A, in the presence of oxalate the current at the membrane electrode does not increase above the background.

Figure 3-22. Cyclic voltammograms of oxalate oxidase membrane electrode: (A) in the absence (——) and in the presence (----) of 2.43 mM oxalate in 0.05 M, pH 3.5 succinate buffer and (B) in the absence (——) and in the presence (----) of 4.86 mM oxalate in 0.05 M, pH 3.5 succinate buffer containing 0.65 mM 8-hydroxyquinoline and 1.0 mM EDTA. Scan rate = 5 mV s^{-1}, initial sweep to positive potentials.

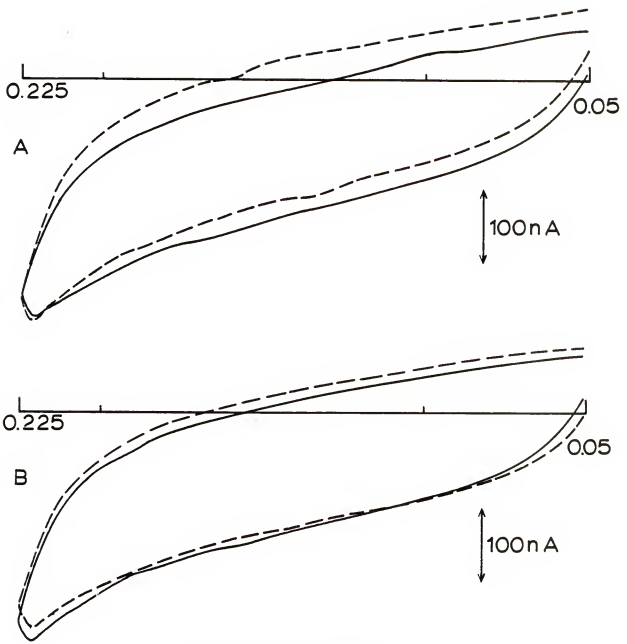
0.225
0.05
A
100nA
0.225
0.05
B
100nA
E(volt) vs SCE

The reported normal values of urinary oxalate in humans are dependent upon the employed measurement methodology (67). In the concentration range which includes the lowest reported normal value of oxalate to ca. 25 times the highest reported upper normal value (1.1×10^{-5} - 4.9×10^{-3} M) (67) the membrane electrode shows no increase in response to oxalate. In oxalate solutions, slow deterioration of the membrane electrode occurs as evidenced by the decrease in current response relative to the blank.

Although it has been reported that the purified enzyme does not need a cofactor and succinate buffer is the only one suitable for oxalate assays (97,98), when 8-hydroxyquinoline and ethylenediaminetetraacetic acid, EDTA, are added to the succinate buffer oxalate oxidase has been reported to exhibit higher enzymatic activity (29,97). The effects of 8-hydroxyquinoline and EDTA have been attributed to their binding of calcium and other metal ions present as impurities. This leads to more free oxalate to be acted upon by the enzyme (79). The membrane electrode response was tested in a 0.05 M, pH 3.5 succinate buffer containing 0.65 mM 8-hydroxyquinoline and 1.0 mM EDTA (79). The results obtained using this buffer system were identical to that observed in the succinate buffer, Figure 3-22B. In either buffer system, no increase in current response at the membrane electrode in the presence of oxalate is observed. These results are consistent with the reported oxygen specificity of this enzyme.

CHAPTER 4
GLUCOSE DEHYDROGENASE MEMBRANE ELECTRODES

The main objective of the work described in this chapter was to develop an amperometric immobilized NAD-dependent enzyme electrode. Several materials were investigated as to their ability to catalyze the direct electrooxidation of NADH. These materials included rough pyrolytic graphite and the conducting organic salts NMP-TCNQ and TTF-TCNQ. The described work deals with the behavior of NADH at these electrode surfaces. Also included is the description of an electrochemical sensor incorporating the NAD-dependent enzyme glucose dehydrogenase and the conducting organic salts into the design. The effect of NADH adsorption on the observed response is examined and will be discussed.

4.1 Electrooxidation of Nicotinamide Adenine Dinucleotide at Rough Pyrolytic Graphite Electrode

Figure 4-1 shows the response of NADH at a RPGE. On the initial sweep to positive potentials, an irreversible oxidation peak is observed at 0.23 V which is ca. 0.55 V more positive than the standard formal potential of NADH oxidation, $E^{0'}$ = -0.32 V versus SCE (117, p. 128). On the subsequent sweep to positive potentials two new oxidation peaks are observed at 0.05 V and 0.32 V, peaks II_a and III_a, respectively. The current of peak III_a decreases upon repetitive cycling reaching a steady-state value on the tenth scan.

Figure 4-1. Cyclic voltammograms of 0.63 mM β-NADH in 0.5 M, pH 7.0 phosphate buffer recorded at RPGE: (A) repetitive scans; (B) first and tenth scans; and (C) supporting electrolyte blank. Scan rate = 100 mV s^{-1}, initial sweeps to positive potentials, electrode area = 0.020 cm^2.

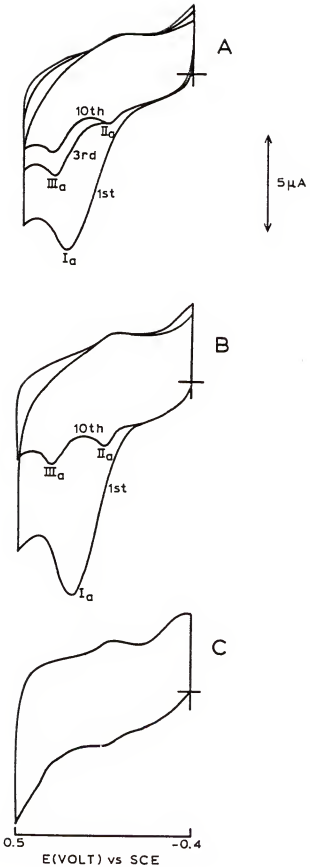
A
10th
IIa
3rd
IIIa
1st
Ia
5μA
B
10th
IIa
IIIa
1st
Ia
C
0.5
-0.4
E(VOLT) vs SCE

The observed electrochemical behavior of NADH is consistent with product adsorption and the concomitant poisoning of the electrode surface. Similar behavior (i.e., electrode poisoning) has been observed at other solid electrodes such as glassy carbon and Pt where the reaction also occurs at considerably higher overpotentials (89,90). Because of the apparent poisoning of the surface, RPG is not suitable as an electrode material incorporating a NAD-dependent enzyme.

4.2 Electrooxidation of Nicotinamide Adenine Dinucleotide at a N-Methylphenazine Tetracyanoquinodimethane Electrode

Figure 4-2 shows the response of NADH at a NMP-TCNQ electrode in the potential range -0.075 to 0.075 V versus SCE. It is clear from Figure 4-2 that the oxidation of NADH is independent of the applied potential. This behavior is in good agreement with that previously reported (37). The potential window in this investigation was chosen because the electrode showed maximum stability and the lowest background in this region.

Figure 4-3 shows the calibration curve at the bare NMP-TCNQ electrode for NADH obtained in 0.1 M Tris-HCl buffer, pH 7.0. The current was measured at +0.075 V versus SCE. The background current obtained in the electrolyte blank was subtracted from the data shown in Figure 4-3. The analytical figures of merit are summarized in Table 4-1. As shown in Figure 4-3 and Table 4-1, the sensitivity at the NMP-TCNQ electrode is good, but the reproducibility of the response is poor. Because of the good sensitivity, an immobilized

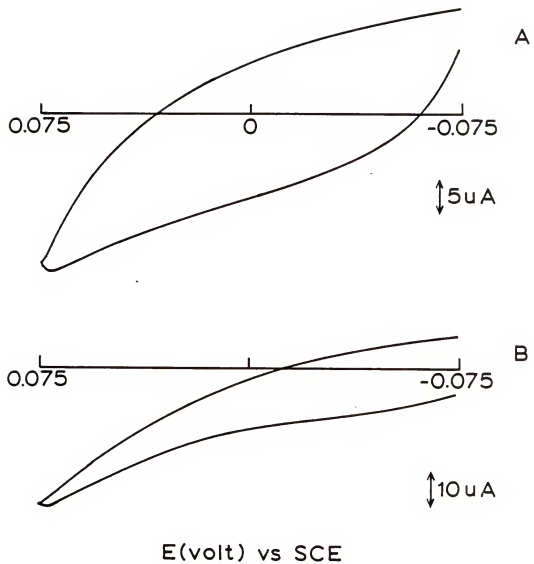

Figure 4-2. Cyclic voltammograms in 0.1 M, pH 7.0 Tris buffer at a NMP-TCNQ electrode in the (A) absence and (B) presence of 0.50 mM β-NADH. Scan rate = 5 mV s^{-1}, initial sweep to positive potentials, electrode area = 0.10 cm^2.

Figure 4-3. Current versus β-NADH concentration response at NMP-TCNQ electrode. Current measured from cyclic voltammograms at +0.075 V versus SCE.

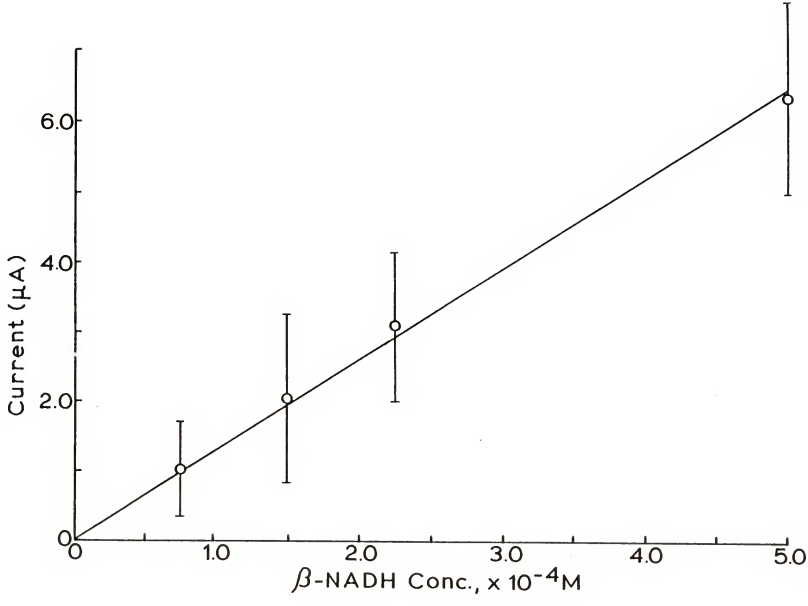
Current (μA)
6.0
4.0
2.0
0
0
1.0
2.0
3.0
4.0
5.0
β-NADH Conc., x 10⁻⁴M

Table 4-1. Response of β-NADH at Organic Conducting Salt Electrodes

electrode material	linear range, M	slope, $\mu A\ mM^{-1}$	intercept, μA	corr. coeff.
NMP-TCNQ[a]	$7.5 \times 10^{-5} - 5.0 \times 10^{-4}$	12.1±2.63	0.01±0.36	0.9975
TTF-TCNQ[b]	$6.0 \times 10^{-5} - 2.1 \times 10^{-4}$	1.92±0.12	-0.03±0.01	0.9940

[a] β-NADH solutions prepared in 0.1 M, pH 7.0 Tris buffer. Currents measured at +75 mV versus SCE from cyclic voltammograms.

[b] β-NADH solutions prepared in 0.5 M, pH 7.0 phosphate buffer. Currents measured at +225 mV versus SCE from cyclic voltammograms.

glucose dehydrogenase amperometric electrode was constructed with NAD as the cofactor.

4.3 Glucose Dehydrogenase Membrane Electrode using N-Methylphenamine Tetracyanoquinodimethane as the Electrode Material

Relative to the flavoenzyme membrane electrodes, the design of the NAD-dependent enzyme electrode is more complex. This increased complexity is due to the difference in the way the redox centers interact with their respective enzymes (31). In the case of the flavoenzymes, the flavin redox center remains bound to the enzyme throughout the catalytic reaction. While for the NAD-dependent enzymes, the NAD-cofactor is free to diffuse away after regenerating the enzyme. Therefore, NAD-cofactor has to be coimmobilized with the enzyme.

The design of the sensor used in this investigation is shown schematically in Figure 4-4. With glucose as the analyte, the following reactions determine the response of the membrane electrode:

$$\text{glucose} + \text{glucose dehydrogenase}_{(ox)} \longrightarrow \text{gluconolactone} + \text{glucose dehydrogenase}_{(red)} \qquad \text{eq. 4.1}$$

$$\text{glucose dehydrogenase}_{(red)} + NAD^+ \longrightarrow \text{glucose dehydrogenase}_{(ox)} + NADH + H^+ \qquad \text{eq. 4.2}$$

$$NADH \longrightarrow NAD^+ + 2e^- + H^+ \qquad \text{eq. 4.3}$$

where reaction 4.3 is expected to occur at the electrode surface. In the initial experiments, an anion exchange membrane was used to trap the enzyme-cofactor solution at the electrode surface. This membrane

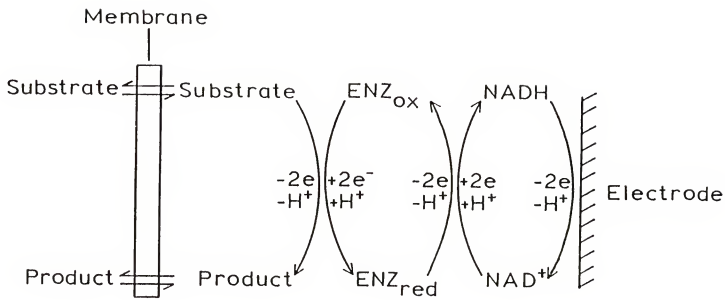

Figure 4-4. Schematic diagram of the NAD-dependent enzyme amperometric membrane electrode.

was employed to prevent the oxidized form of the cofactor from diffusing into the bulk solution.

With this membrane in place, the electrode response never increased over the background current levels. Long incubation times in the presence of glucose (ca. 20 mins.) did not improve the response.

A porous dialysis membrane was also used to immobilize the enzyme-cofactor solution at the electrode surface. The ability of the NAD-cofactor to diffuse through the dialysis membrane was evaluated using spectroscopy. A 1.5 mM solution of NADH in 0.1 M Tris-HCl buffer, pH 7.0 was dialyzed against the buffer. After 24 hours, the dialyzed NADH solution showed a decrease in absorbance at 340 nm of only 5%. It was, therefore, concluded that NADH did not diffuse through the dialysis membrane at an appreciable rate to preclude its use for immobilization purposes.

Figure 4-5 shows the working curve obtained at this membrane electrode. As shown in Figure 4-5, an increase in current is observed at low concentrations of glucose. At higher concentrations, the response decreases. During the course of these measurements, the blank readings also decreased in a manner that paralleled the behavior shown in Figure 4-5. The decrease in oxidation current has been reported for the electrooxidation of NADH at glassy carbon and silver electrodes (90,128). The cause of this behavior has been postulated as being the polymerization of some oxidation products at the electrode surface (116), and electrode fouling has been circumvented by using lower concentrations of NADH (116). Therefore,

Figure 4-5. Calibration curve for glucose at glucose dehydrogenase membrane electrode. Membrane electrode prepared by coimmobilizing 1.5 mM NAD and 32 μM glucose dehydrogenase at NMP-TCNQ electrode. Steady-state response measured at +0.075 V versus SCE.

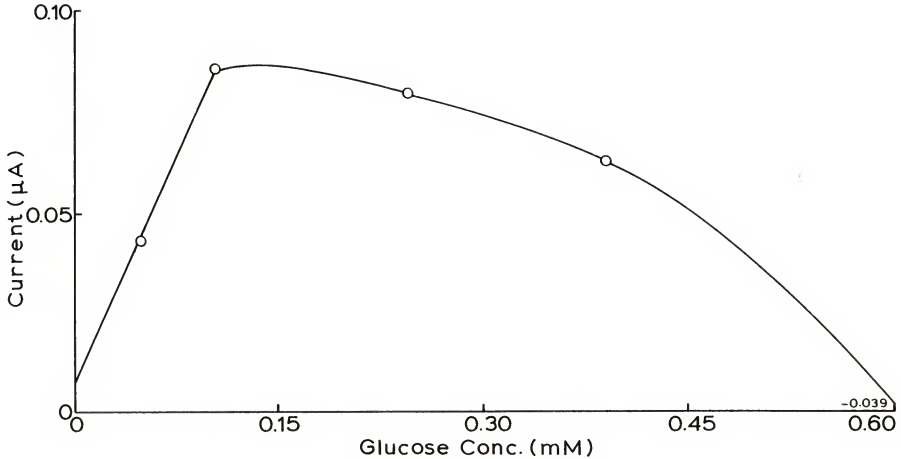
0.10
0.05
0
Current (μA)
-0.039
0
0.15
0.30
0.45
0.60
Glucose Conc. (mM)

the above experiments were repeated using a lower concentration of NAD-cofactor (0.15 mM) trapped at the electrode surface. As shown in Figure 4-6, a response similar to that shown in Figure 4-5 is obtained. The blank readings showed a current decrease in the same manner as was observed at higher NAD concentrations. It was, therefore, concluded that a decrease in sensitivity of the NMP-TCNQ electrode was occurring at high and low concentrations of NAD.

As a means of achieving a stable and reproducible response, pretreatment of the NMP-TCNQ electrode surface with NADH was attempted. It has been reported that the flavin redox center of glucose oxidase could be adsorbed onto an electrode surface, and when the apoenzyme was added enzymatic activity was obtained (113). With this approach in mind, attempts were made to adsorb NADH to the surface of the electrode followed by immobilization of the enzyme.

The bare NMP-TCNQ electrode was placed in 1.5 mM NADH for ca. 30 mins. at an open circuit. A thin layer of glucose dehydrogenase without NAD-cofactor was trapped at the electrode surface. The electrode prepared in this manner showed no response in the presence of glucose. It is possible that not enough NADH was adsorbed to the electrode surface to cause a response. It was argued that the gradual passivation of the electrode by NADH could be the source of the decreased sensitivity. Therefore, an attempt was made to form such a coating on the electrode surface and then immobilize the cofactor and the enzyme. Such precoating was shown to be effective to maintain the stability of graphite electrodes (35,113). Thus, the electrode was placed in a 1.5 mM NADH solution and was poised at

Figure 4-6. Calibration curve for glucose at glucose dehydrogenase membrane electrode in 0.1 M, pH 7.0 Tris buffer. Membrane electrode prepared by coimmobilizing 0.15 mM NAD and 32 μM glucose dehydrogenase at NMP-TCNQ electrode. Steady-state response measured at +0.075 V versus SCE.

0.03
0.02
0.01
Current (μA)
0.0
2.0
4.0
6.0
8.0
10.0
Glucose Conc. (mM)

+0.075 V, where the electrooxidation of NADH occurs, for ca. 15 min. A thin layer of the enzyme-cofactor solution was immobilized at the surface of this pretreated electrode. With this membrane electrode the background current stabilized; however, the method of stabilization considerably decreased the sensitivity of the membrane electrode as shown in Figure 4-7.

Due to the difficulties associated with product adsorption and poor stability, it was concluded that NMP-TCNQ is not suitable as an electrode material in the construction of the sensor shown in Figure 4-1.

4.4 Electrooxidation of Nicotinamide Adenine Dinucleotide at Tetrathiafulvalene Tetracyanoquinodimethane and Tetrathiafulvalene Tetracyanoquinodimethane Membrane Electrode

Flavins are known to react slowly with NADH in homogeneous solutions (91). Since flavins react at TTF-TCNQ electrodes it was postulated that NADH may also react at TTF-TCNQ. Thus, TTF-TCNQ was evaluated as an electrode material for the electrooxidation of NADH. Figure 4-8 shows the response of NADH at a TTF-TCNQ electrode. As shown in Figure 4-8, the rate of NADH oxidation is potential independent in the range of +0.10 to 0.40 V versus SCE similar to the behavior observed at NMP-TCNQ. Figure 4-9 shows the typical working curve obtained at a TTF-TCNQ electrode. It is evident that the reproducibility achieved with TTF-TCNQ electrode is better compared to that at a NMP-TCNQ electrode. However, the sensitivity (Table 4-1) at the TTF-TCNQ electrode is considerably lower which may account for the higher reproducibility. The better

Figure 4-7 Current versus glucose concentration response at a glucose dehydrogenase membrane electrode in 0.1 M, pH 7.0 Tris buffer. N-Methylphenazine tetracyanoquinodimethane electrode electrochemically pretreated with 0.15 mM β-NADH for 30 min. Membrane electrode prepared by coimmobilizing 0.15 mM NAD and 32 μM glucose dehydrogenase at pretreated NMP-TCNQ electrode. Steady-state response measured at +0.075 V versus SCE.

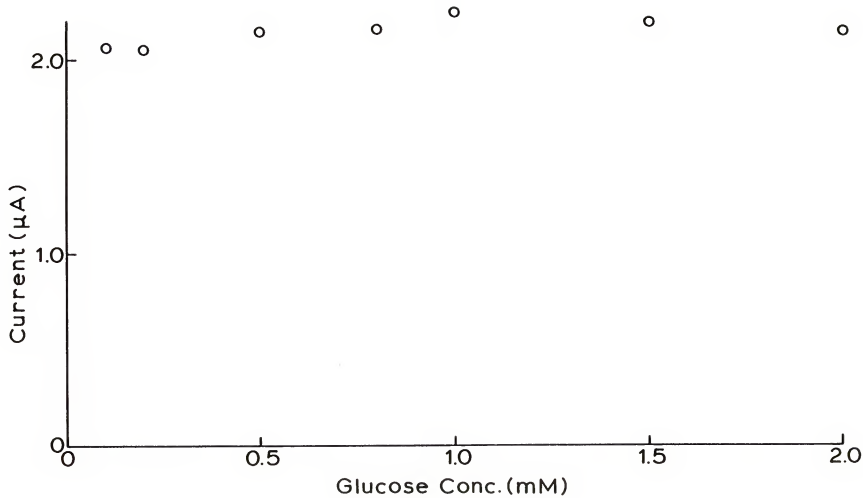
Current (μA)
2.0
1.0
0
0
0.5
1.0
1.5
2.0
Glucose Conc. (mM)

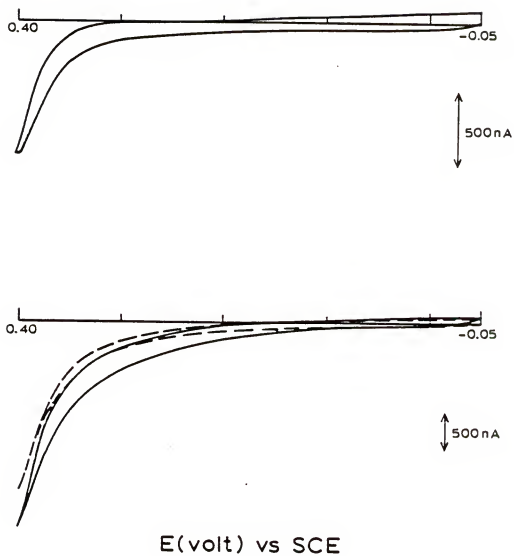

Figure 4-8. Cyclic voltammograms in 0.5 M, pH 7.0 phosphate buffer at a TTF-TCNQ electrode in the (A) absence and in the (B) presence of 0.64 mM β-NADH (---) tenth scan. Scan rate = 5 mV s^{-1}, initial sweeps to positive potentials.

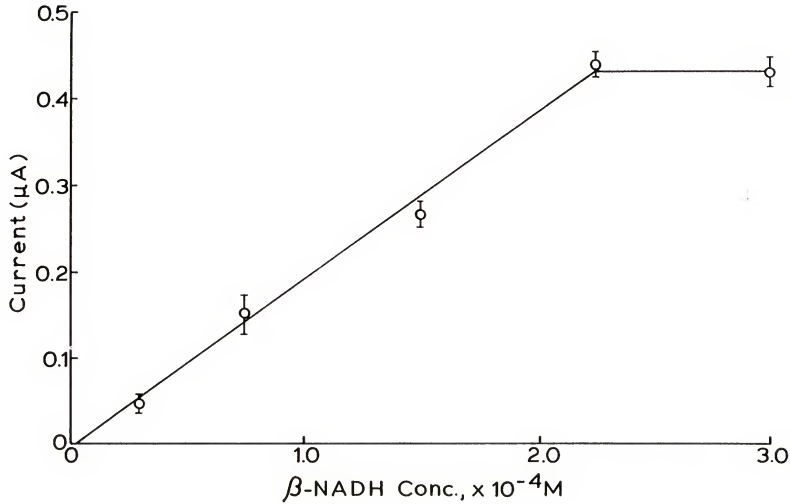

Figure 4-9. Current versus β-NADH concentration response at a TTF-TCNQ electrode in 0.5 M, pH 7.0 phosphate buffer. Currents measured from cyclic voltammograms at +0.225 V versus SCE.

reproducibility at TTF-TCNQ may be caused by a larger potential window which limits lattice oxidation at analytical potentials compared to that at NMP-TCNQ (50).

A membrane electrode was constructed using TTF-TCNQ as the electrode material. A thin layer of the enzyme and 0.15 mM of the NAD-cofactor was trapped at the electrode surface using the porous dialysis membrane. When tested in a glucose concentration range of 1×10^{-5} to 1×10^{-2} M, the response of the membrane electrode did not increase over the background current. Trapping the enzyme at the electrode surface undoubtably decreased the effective electrode area which may have led to a decrease in the active surface area at which the NADH could react. This coupled with the initial poor sensitivity of the bare electrode was probably the cause of this behavior. Hence it was concluded that although TTF-TCNQ showed improved reproducibility, its lack of sensitivity prevented its use as an electrode material in the construction of the sensor shown in Figure 4-4.

CHAPTER 5
ELECTROCHEMICAL BEHAVIOR OF SMALL BIOLOGICAL MOLECULES AT TETRATHIAFULVALENE TETRACYANOQUINODIMETHANE ELECTRODES IN AQUEOUS MEDIA

Tetrathiafulvalene tetracyanoquinodimethane and N-methylphenazine tetracyanoquinodimethane have demonstrated value in improving the heterogeneous kinetics by reducing the overpotential in the catalytic oxidation of a flavoenzyme and NADH. The nature of this catalysis is a subject of debate (22,23). At the TTF-TCNQ electrodes used in this study, ferrocyanide oxidation in pH 7.0 phosphate buffer occurs at the same potential as that reported by Jaeger and Bard at TTF-TCNQ disk electrodes prepared at high pressures (49). The reduction peak occurs at more negative potentials and ΔE_p = 120 mV (compared to ca. 50 mV reported by Jaeger and Bard) (49). This suggests that the method of electrode preparation has control over reactivity. The work reported in this chapter was aimed at gaining insight into the reactivity of structurally different molecules at TTF-TCNQ electrodes. In this investigation, biological molecules of analytical interest which show different sensitivity to surface conditions were investigated, and the analytical utility of TTF-TCNQ electrodes in the determination of these compounds is also addressed.

5.1 Oxidation of 6-Thiopurines

The cyclic voltammogram of 6-mercaptopurine, 6-MP, at a TTF-TCNQ electrode is shown in Figure 5-1A. It appears from this voltammogram

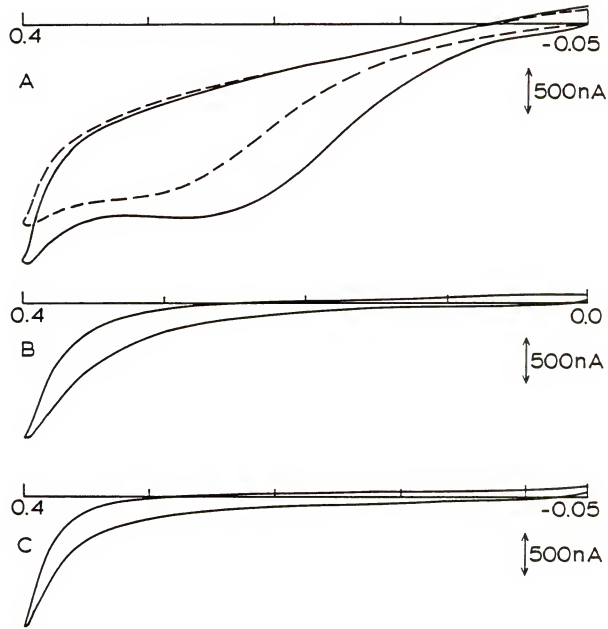

Figure 5-1. Cyclic voltammograms of 6-thiopurines in 0.5 M, pH 8.0 phosphate buffer at a TTF-TCNQ electrode: (A) 0.50 mM 6-mercaptopurine (---) tenth scan; (B) 0.49 mM 6-thioxanthine; and (C) supporting electrolyte blank. Scan rate = 5 mV s^{-1}, initial sweeps to positive potentials.

that 6-MP starts to oxidize at ca. 0.10 V and the peak current reaches a maximum at ca. 0.26 V versus SCE. The current is greater than that of the electrode blank at 0.4 V.

At a RPGE, the cyclic voltammogram of 6-MP in pH 8.0 phosphate buffer, ionic strength 0.5 M shows a well-defined oxidation peak at 0.2 V versus SCE. A plot of peak current versus 6-MP concentration is nonlinear, and the plot of log peak current versus log scan rate has a slope of 0.7 at low concentration (0.5 mM). At higher concentrations (1.7 mM), the log peak current versus log scan rate plot has a slope of 0.8. Hence at both low and high concentrations, the oxidation of 6-MP shows a mixed adsorption-diffusion controlled behavior. A plot of peak current versus 6-MP concentration at a TTF-TCNQ electrode exhibits no breaks in linearity. The analytical figures of merit are summarized in Table 5-1. On repetitive cycling the response shows a 16% change in sensitivity, Figure 5-1A. An attempt to determine the dependence of i_{max} on scan rate was not successful because of high background noise at higher scan rates which may be the result of poor electrical contact inherent in the design of the electrode.

The cyclic voltammogram of 6-thioxanthine, 6-TX, at a TTF-TCNQ electrode is shown in Figure 5-1B. The cyclic voltammogram shows no oxidation or reduction peaks. A slight increase in current is measurable at 0.4 V relative to the supporting electrolyte blank. In contrast, in pH 8.0 phosphate buffer at a RPGE, 6-TX shows two oxidation peaks. Peak I_a occurs at 0.34 V and peak II_a has a peak potential of 0.70 V. The plot of log peak I_a current versus log scan

Table 5-1. Response of Small Biological Molecules at TTF-TCNQ Electrodes

compound	linear range[b], M	slope, $\mu A\ mM^{-1}$	intercept, μA	corr. coeff.
purine	NR[a]			
hypoxanthine	NR[a]			
xanthine	NR[a]			
uric acid[b]	2.9×10^{-5} - 1.5×10^{-3}	1.58±0.06	0.040±0.03	0.9977
6-thioxanthine[b]	2.4×10^{-4} - 6.4×10^{-3}	0.10±0.002	0.028±0.005	0.9990
6-mercapto-purine[b]	5.0×10^{-5} - 1.0×10^{-3}	3.37±0.14	-0.11±-0.08	0.9965
ascorbic acid[c]	3.3×10^{-5} - 1.6×10^{-3}	6.53±0.15	0.074±0.12	0.9971

[a] No response.

[b] Results obtained in 0.5 M phosphate buffer, pH 8.0.

[c] Results obtained in 0.5 M phosphate buffer, pH 7.0.

[d] Current measured at 0.225 V versus SCE; electrode material TTF-TCNQ.

rate has a slope of 0.9 at low (0.13 mM) and high (0.90 mM) concentrations (25). This, together with the nonlinear dependence of peak I_a current on 6-TX concentration, indicates that 6-TX is adsorbed at RPGE at this potential. A plot of peak current versus 6-TX concentration can be obtained at a TTF-TCNQ electrode at 0.4 V. It shows poor sensitivity, but linearity is observed through the concentration range 2.4×10^{-4} to 9.0×10^{-3} M. The analytical figures of merit are summarized in Table 5-1.

5.2 Oxidation of Biological Purines

The oxidation of biological purines at a TTF-TCNQ electrode was investigated because these compounds represent excellent models of electroactivity of small biological molecules. They are also of considerable analytical interest, and in addition their electrochemical behavior is well characterized (129, pp. 71-80).

As can be expected, no catalytic oxidation of xanthine, hypoxanthine and purine was observed in the stable potential window of a TTF-TCNQ electrode. The response of uric acid at a TTF-TCNQ electrode is shown in Figure 5-2B. The electrochemical oxidation of uric acid is known to be a 2e, $2H^+$ process, and the oxidation product has been shown to rapidly hydrate (K_{app} = 30 s at pH 8.0) (118). The product can be stabilized by adsorption at RPGE (118). From the obtained cyclic voltammetric results at RPGE the 2 e formal potential of uric acid at pH 8.0 can be estimated as $E^{0'} = 0.240 \pm 0.10$ V.

Figure 5-2B shows that the oxidation of uric acid at the TTF-TCNQ electrode is irreversible. The oxidation at pH 8.0 reaches

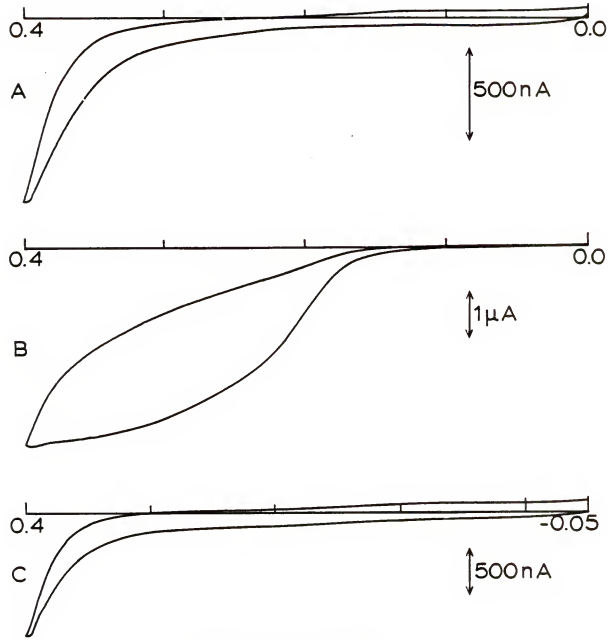

Figure 5-2. Cyclic voltammograms of purines in 0.5 M, pH 8.0 phosphate buffer at a TTF-TCNQ electrode: (A) 0.49 mM xanthine; (B) 0.53 mM uric acid; and (C) supporting electrolyte blank. Scan rate = 5 mV s^{-1}, initial sweep to positive potentials.

a maximum rate, as indicated by the inflection point in the cyclic voltammetric curve, at ca. 0.230 V versus SCE, occurring close to the $E^{0'}$ value for the 2 e process. The background current at 0.40 V increases substantially, and the peak has a flat-topped shape. The linear response to uric acid at a TTF-TCNQ electrode over a wide concentration range (Table 5-1) and the stability of the response upon repetitive cycling indicates that the reactant adsorption at this electrode is not significant.

5.3 Oxidation of Dopamine and Ascorbic Acid

The oxidation of dopamine and ascorbic acid has been extensively studied at different surfaces because of considerable interest in their simultaneous detection (6,7). The structures of dopamine and ascorbic acid are shown in Figure 5-3. At most surfaces ascorbate oxidation is irreversible (130). However, at heat-treated glassy carbon electrodes at pH 7.0 oxidation occurs at 0.0 V versus SCE close to the 2 e formal potential ($E^{0'}$ = -0.061 V versus SCE) (130). A similar oxidation potential is observed at RPGE ($E^{0'}$ = -0.013 V versus SCE, pH 8.0), Figure 5-4B.

At a TTF-TCNQ electrode, the ascorbic acid oxidation peak occurs at 0.127 ± 0.023 V, Figure 5-5A. From the ca. +100 mV shift in peak potential, it can be estimated (130) that the oxidation is ca. 7 times slower at TTF-TCNQ than at RPGE. On both the RPGE and TTF-TCNQ electrodes, the oxidation of ascorbic acid is irreversible.

The electrochemical behavior of dopamine is also a function of the condition of the electrode surface (131). At "active" surfaces

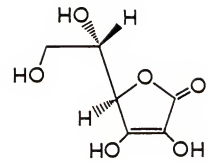

A. Ascorbic Acid

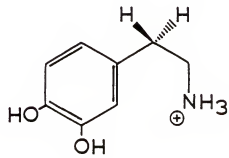

B. Dopamine

Figure 5-3. Structure of ascorbic acid and dopamine.

Figure 5-4. Cyclic voltammograms at a RPGE: (A) 0.5 M, pH 7.0 phosphate buffer; (B) 1.4 mM ascorbic acid; (C) 0.51 mM dopamine; and (D) 0.49 mM ascorbic acid plus 0.30 mM dopamine. Scan rate = 100 mV s^{-1}, initial sweeps to positive potentials.

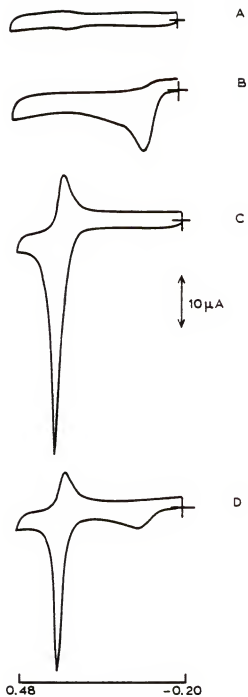
A
B
C
10μA
D
0.48
-0.20
E(VOLT) vs SCE

Figure 5-5. Cyclic voltammograms at a TTF-TCNQ electrode: (A) 1.4 mM ascorbic acid; (B) 0.51 mM dopamine; (C) 0.49 mM ascorbic acid plus 0.30 mM dopamine; and (D) 0.5 M, pH 7.0 phosphate buffer. Scan rate = 5 mV s^{-1}, initial sweeps to positive potentials.

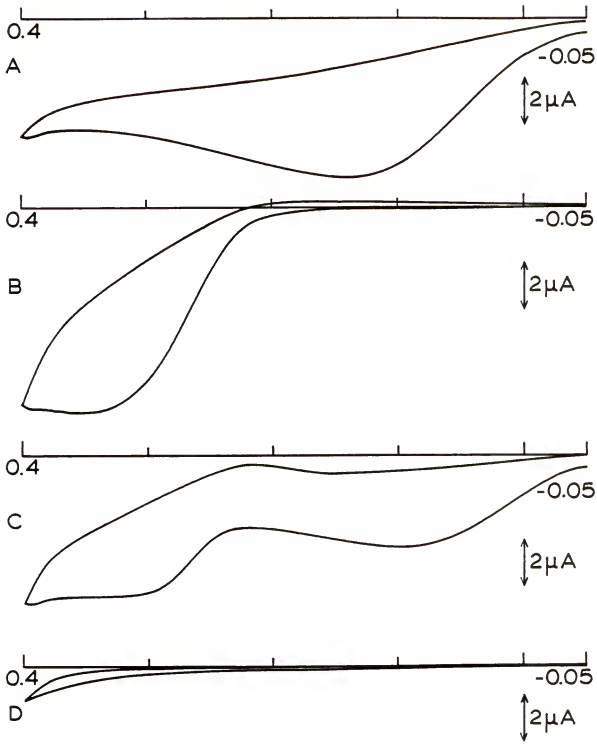
0.4
A
-0.05
2μA
0.4
-0.05
B
2μA
0.4
C
-0.05
2μA
0.4
-0.05
D
2μA
E(volt) vs SCE

the behavior is quasi-reversible ($k_s = 10^{-3}$ cm s^{-1}, pH 7.4) (132), and adsorption of dopamine and its oxidation product is observed (131,133). The oxidation product is unstable in homogeneous solution ($t_{1/2}$ = 5 s) (134). From results obtained at RPGE at pH 8.0 the formal potential for the 2 e process was estimated at $E^{0'}$ = +0.298 V versus SCE, Figure 5-4C.

Figure 5-5B shows the response of dopamine at a TTF-TCNQ electrode in pH 7.0 phosphate buffer. The oxidation current starts to increase at ca. 0.23 V and reaches a maximum at 0.35 V versus SCE. As shown in Figure 5-5B, the oxidation of dopamine at TTF-TCNQ electrode is irreversible. The oxidation peak potential at a TTF-TCNQ electrode is ca. 40 mV more positive than at the RPGE (E_{Pa} = 0.321 V).

Figure 5-5C shows the response at a TTF-TCNQ electrode obtained in a solution containing both dopamine and ascorbic acid. As is clear from this result ascorbic acid can easily be detected in the presence of dopamine. This frequently is a problem because, although it is thermodynamically easier to oxidize ascorbic acid than dopamine, the peak potential for ascorbic acid is more positive than dopamine (117, p. 121). It has been reported that oxidation of dopamine at carbon electrodes in the presence of ascorbic acid results in a homogeneous catalytic oxidation of ascorbic acid (132). As a result dopamine is regenerated and returns to the electrode to give an enhanced current. The catalytic rate for this reaction is fast enough that it is difficult to resolve voltammetric waves for dopamine and ascorbic acid in the presence of one another

at carbon electrodes (132). The presence of a small reduction peak following dopamine oxidation may be the result of a mediated reaction between ascorbate and the oxidation product of dopamine (132). Such a reaction can lead to continuous chemical regeneration of dopamine and, under some conditions, to the possible accumulation of the dopamine oxidation product near the electrode. Since the reverse peak is not present in the dopamine solution alone (Figure 5-5B), this suggests that the oxidation product is not stabilized through adsorption.

The reactivity of small biological compounds investigated in this study is increased at the TTF-TCNQ electrodes compared to that at nonactivated graphite. Compared to the behavior at RPGE which is an "active" surface, as is clear from the ascorbic acid oxidation potential, the behavior at TTF-TCNQ is less reversible. A clear advantage of these electrodes is the relative freedom from electrode poisoning, as indicated by the repetitive cycling experiments and the wide linear dynamic range.

CHAPTER 6
SUMMARY AND FUTURE WORK

The purpose of this research was to investigate the behavior of immobilized enzyme electrodes constructed using conducting organic salts as the electrode materials. In this work, it was shown that a xanthine oxidase membrane electrode constructed using TTF-TCNQ as the electrode material could be applied to the analysis of the biological purines: xanthine, hypoxanthine and purine in blood plasma. The major advantage of using this salt as the electrode material is the simplicity by which the enzyme is regenerated. Following the specific enzyme-analyte reaction, the analytical signal is produced by the direct transfer of electrons from the enzyme to the electrode itself. The mechanism by which this electron transfer takes place is unknown at this time and further work is needed before one can be proposed.

The kinetics of the xanthine oxidase membrane electrode were analyzed using theories developed by Albery and Bartlett (120) and Mell and Maloy (126). The results obtained utilizing both of these approaches identify substrate diffusion through the membrane as being the rate-limiting step. Analytically, this is the most desirable situation since the electrochemical and enzymatic kinetics are fast by comparison and, therefore, do not affect the electrode response.

Of particular interest in Table 3-5 is the observation that for large values of V (equation 3.26), the linear range of the amperometric response of the membrane electrode is shown to extend beyond the K_M values for the enzymatic reactions in homogeneous solutions. As shown in Table 3-5, the greatest value of V corresponds to the largest increase in the apparent Michaelis-Menten constant, K_{ME}. However, as shown in Tables 3-2 and 3-5, there is an inverse relationship between the value of V and the observed sensitivity of the membrane electrode. The magnitude of V is directly proportional to the membrane thickness (equation 3.26), and as a result of this relationship, the linear range and sensitivity of the membrane electrode can be optimized for a particular analysis by judiciously choosing the membrane thickness.

Of the two theories used in the kinetic analysis of the membrane electrode response, the one developed by Albery and Bartlett was more quantitative. Rate constants are obtained for the electrochemical, enzymatic and diffusional processes by constructing a series of diagnostic plots (equations 3.13 and 3.17). In comparison, the theory of Mell and Maloy was qualitative, and although the rate-limiting step is identified, no additional information is obtained, e.g., apparent Michaelis-Menten constant, K_{ME}.

In Chapter 3, it was reported that 6-thioxanthine reacts at a bare TTF-TCNQ electrode, Table 3-1. In subsequent experiments, it was found this response was a result of the electrode history, and, therefore, the response of 6-thioxanthine at a xanthine oxidase membrane electrode should be reevaluated.

Oxalate oxidase did not undergo direct electrooxidation at the TTF-TCNQ electrode. Efforts to induce the electrooxidation by using a different medium to enhance enzymatic activity proved to be unsuccessful. Previous work with other alternative oxidants has shown this enzyme to be specific for oxygen as the acceptor and, thus, the observed results are consistent with these findings. However, correlation between reactivity at TTF-TCNQ electrodes and the flavoenzyme's electron acceptor specificity should not be attempted based on this study alone. Recently, Albery and coworkers have reported that choline oxidase, a flavoenzyme of high electron acceptor specificity, undergoes direct electrooxidation at a TTF-TCNQ electrode (24). Therefore, each flavoenzyme should be evaluated as to its reactivity at a conducting organic salt electrode regardless of its reported electron acceptor specificity in homogeneous solution.

Glucose levels in body fluids are currently measured using glucose oxidase enzyme electrodes which detect the endproduct of the enzymatic reaction (2, pp. 94-97). The design of this and other immobilized flavoenzyme electrodes used in commercial instruments can be simplified by using TTF-TCNQ as the electrode material. In the case of xanthine oxidase membrane electrode, the poor lifetime of the enzyme would prevent its routine use in analysis of purines. The stability of the enzyme might be improved by covalently binding it to the TTF-TCNQ electrode surface.

It was also shown that the overpotential for NADH oxidation at RPG, NMP-TCNQ and TTF-TCNQ electrodes can be reduced relative to that

observed at untreated carbon and noble metal electrodes. However, as is the case with the latter electrodes RPG and NMP-TCNQ electrode surfaces are fouled by the NADH oxidation product leading to poor reproducibility. Means of preventing this electrode poisoning need to be investigated before electrochemical sensors incorporating NAD-dependent enzymes can be developed. One possible means towards this end is to bring about the irreversible binding of the NAD cofactor to the enzyme. This may prevent the fouling of the electrode by the NADH oxidation product since the NAD cofactor would be intimately bound to the large protein molecule. The NADH oxidation at TTF-TCNQ electrodes shows increased reproducibility but poorer sensitivity. The exact mechanism by which NADH reacts at these electrodes is unknown and further work is needed to elucidate this process.

The reactivity of small biological compounds at TTF-TCNQ electrodes was investigated and compared to that observed at RPG electrodes. It was found that the rate of electrochemical oxidation of these compounds can be increased at TTF-TCNQ relative to untreated carbon electrodes. However, the electrochemical behavior of these compounds at TTF-TCNQ was less reversible, as evidenced by the observed behavior of ascorbic acid, than that observed at RPGE. Double layer capacitance measurements at the TTF-TCNQ electrode reveal that the electrode acts as a polarizable electrode in the reported potential window, but the exact electron transfer mechanism between the electrode and the compounds is unknown. Further work would prove useful in providing insight into this mechanism.

As shown in Chapter 5, detection of dopamine in the presence of ascorbic acid is possible at TTF-TCNQ electrodes. This property coupled with the ease by which single crystals can be grown is of potential usefulness in the in vivo measurements of neurotransmitters. Another clear advantage of these salts is the relative freedom from electrode poisoning, as indicated by the wide linear dynamic range.

REFERENCES

1. Czaban, J.D., Anal. Chem., 1985, 57, 345A.

2. Evenson, M.A., In "Clinical Diagnosis and Management by Laboratory Methods"; Henry, J.B., Ed.; W.B. Saunders Company: Philadelphia, 1979.

3. Osteryoung, J.G.; Osteryoung, R.A., Anal. Chem., 1985, 57, 101A.

4. Stojek, I.; Osteryoung, J.G., Anal. Chem., 1981, 53, 847.

5. Osteryoung, J.G., J. Chem. Ed., 1983, 60, 296.

6. Adams, R.N., Anal. Chem., 1976, 48, 1127A.

7. Wightman, R.M., Anal. Chem., 1981, 53, 1125A.

8. Clevett, K.J., "Handbook of Process Stream Analysis"; Halsted Press: New York, 1974.

9. Murray, R.W., "Electroanalytical Chemistry, Vol. 13"; Bard, A.J., Ed.; Marcel Dekker: New York, 1984.

10. Murray, R.W.; Ewing, A.G.; Durst, R.A., Anal. Chem., 1987, 59, 379A.

11. Carr, P.W.; Bowers, L.D., "Immobilized Enzymes in Analytical and Clinical Chemistry"; John Wiley and Sons: New York, 1980.

12. Guilbault, G.G., "Enzymatic Methods of Analysis"; Pergamon: New York, 1970.

13. Bowers, L.D.; Carr, P.W., Anal. Chem., 1976, 48, 545A.

14. Rechnitz, G.A., Anal. Chem., 1982, 54, 1982.

15. Updike, S.J.; Hicks, G.P., Nature, 1967, 214, 986.

16. Lobel, E.; Resfon, J., Anal. Chem., 1981, 53, 51.

17. Clark, L.C., "Biotechnology and Bioengineering Symposium No. 3"; John Wiley and Sons: New York, 1972.

18. Ianniello, R.M.; Lindsay, T.J.; Yacynych, A.M., Anal. Chem., 1982, 54, 1980.

19. Cass, A.E.G.; Davis, G.; Francis, G.D.; Hill, H.A.O.; Aston, W.J.; Higgins, I.J.; Plotkin, E.V.; Scott, L.D.L.; Turner, A.P.T., Anal. Chem., 1984, 56, 662.

20. Cass, A.E.G.; Davis, G.; Green, M.J.; Hill, H.A.O., J. Electroanal. Chem., 1985, 190, 117.

21. Kulys, J.J.; Samalius, A.S.; Svimichas, G.J.S., FEBS Lett., 1980, 114, 7.

22. Cenas, N.; Kulys, J., Bioelectrochem. Bioenerg., 1980, 8, 103.

23. Albery, W.J.; Bartlett, P.N.; Craston, D.H., J. Electroanal. Chem., 1985, 194, 223.

24. Albery, W.J.; Bartlett, P.N.; Bycroft, M.; Craston, D.H.; Driscoll, B.J., J. Electroanal. Chem., 1987, 218, 119.

25. McKenna, K.; Brajter-Toth, A., J. Electroanal. Chem., in press.

26. Bergmann, F.; Levene, L., Biochem. Biophys. Acta, 1976, 429, 672.

27. Barman, T.E., "Enzyme Handbook, Vol. 1"; Springer-Verlag, New York, 1969.

28. Massey, V., In "Iron-Sulfur Proteins"; Lovenberg, W., Ed.; Academic Press: New York, 1983.

29. Chiriboga, J., Arch., Biochem. Biophys., 1966, 116, 516.

30. Hodgkinson, A., Clin. Chem., 1970, 16, 547.

31. Walsh, C., Acc. Chem. Res., 1980, 13, 148.

32. Rawn, J.D., "Biochemistry"; Harper and Row: New York, 1983.

33. Gorton, L.; Johansson, G., Anal. Chem., 1981, 53, 1979.

34. Gorton, L.; Johansson, G., J. Electroanal. Chem., 1984, 161, 103.

35. Gorton, L.; Johansson, G.; Torstensson, T.E., Anal. Chim. Acta, 1986, 179, 371.

36. Degrand, C.; Miller, L.L., J. Am. Chem. Soc., 1980, 102, 5728.

37. Albery, W.J.; Bartlett, P.N., J. Chem. Soc. Chem. Comm., 1984, 234.

38. Babson, A.L.; Babson, S.R., Clin. Chem., 1973, 19, 766.

39. Albery, W.J.; Bartlett, P.N.; Cass, A.E.G.; Sim, K.W., J. Electroanal. Chem., 1987, 218, 127.

40. Acker, D.S.; Harder, R.J.; Hertler, W.R.; Mahler, W.; Melby, L.R.; Benson, R.E.; Mochel, W.E., J. Am. Chem. Soc., 1960, 82, 6408.

41. Wudl, F.; Smith, G.M.; Hufnagel, E.J., J. Chem. Soc. Comm., 1970, 1453.

42. Wudl, F.; Wobschall, D.; Hufnagel, E.J., J. Am. Chem. Soc., 1972, 94, 670.

43. Ferraris, J.; Cowan, D.O.; Walatka, V.; Perlstein, J.H., J. Am. Chem. Soc., 1973, 95, 948.

44. Coleman, L.E.; Cohen, J.A.; Gauto, A.F.; Huger, A., J. Phys. Rev., 1973, B7, 2122.

45. Bryce, M.R.; Murphy, L.C., Nature, 1984, 309, 119.

46. Bechgaard, K.; Jerome, D., Sci. American, 1982, 247, 52.

47. Greene, R.L.; Street, G.B., Science, 1984, 226, 651.

48. Cowan, D.; Wrygul, F.M., C + EN, 1986, July, 21, 28.

49. Jaeger, C.D.; Bard, A.J., J. Am. Chem. Soc., 1979, 101, 1690.

50. Jaeger, C.D.; Bard, A.J., J. Am. Chem. Soc., 1980, 102, 5435.

51. Henning, T.P.; White, H.S.; Bard, A.J., J. Am. Chem. Soc., 1981, 103, 3937.

52. Schroeder, A.H.; Kaufman, F.B.; Platel, V.; Engler, E.M., J. Electroanal. Chem., 1980, 113, 193.

53. Schroeder, A.H.; Kaufman, F.B., J. Electroanal. Chem., 1980, 113, 209.

54. Kaufmann, F.B.; Schroeder, A.H.; Engler, E.M.; Kramer, S.R.; Chambers, J.Q., J. Am. Chem. Soc., 1980, 102, 483.

55. Inzelt, G.; Kaufmann, F.B.; Chambers, J.Q., J. Electroanal. Chem., 1983, 159, 443.

56. Lange, M.A.; Day, R.W.; Kinstle, J.F.; Chambers, J.Q., Anal. Chem., 1984, 56, 301.

57. Inzelt, G.; Chambers, J.Q.; Kinstle, J.F.; Day, R.W., J. Am. Chem. Soc., 1984, 106, 3396.

58. Houshang, K.; Chambers, J.Q., J. Electroanal. Chem., 1987, 217, 313.

59. Lehninger, A.L., "Biochemistry"; Worth Publisher, Inc.: New York, 1975.

60. Chalmers, R.A.; Watts, R.W.E., Analyst, 1968, 93, 354.

61. Chalmers, R.A.; Watts, R.W.E., Analyst, 1969, 94, 226.

62. Hayashi, T.T.; Gilling, B., Anal. Biochem., 1970, 36, 343.

63. Sweetman, L.; Nyhan, W., Anal. Biochem., 1969, 31, 358.

64. Assenza, S.P.; Brown, P., J. Chromatogr., 1983, 282, 477.

65. McCloskey, J.A., In "Basic Principles in Nucleic Acid Chemistry, Vol. 1"; Ts'O, P.O., Ed.; Academic Press: New York, 1974.

66. White, E.; Krueger, V.P.M.; McCloskey, J.A., J. Org. Chem., 1972, 37, 430.

67. Zervekh, J.E.; Drake, E.; Gregory, J.; Griffith, D.; Hofmann, A.F.; Menon, M.; Pak, C.Y.C., Clin. Chem., 1982, 29, 1977.

68. Zarembski, P.M.; Hodgkinson, A., Analyst, 1962, 87, 698.

69. Archer, H.E.; Dormer, A.E.; Scowen, E.F.; Watts, R.W.E., Clin. Sci., 1957, 16, 405.

70. Hausman, E.R.; McAnally, J.S.; Lewis, G.T., Clin. Chem., 1956, 2, 439.

71. Vittu, C.; Lemahieu, L., Ann. Biol. Clin., 1965, 23, 913.

72. Powers, H.H.; Levatin, P., J. Biol. Chem., 1944, 154, 207.

73. Dodds, E.C.; Gallimore, E.J., Biochem. J., 1932, 26, 1242.

74. Pik, C.; Kerckhoff, H.P.M., Clin. Chem. Acta, 1963, 8, 300.

75. Dean, B.M.; Griffin, W.J., Nature, 1965, 205, 598.

76. Hatch, M.; Bourke, E.; Costello, J., Clin. Chem., 1977, 23, 76.

77. Laker, M.F.; Hofmann, A.F.; Meeuse, B.J.D., Clin. Chem., 1980, 26, 827.

78. Kobos, R.K.; Ramsey, T.A., Anal. Chim. Acta, 1980, 121, 111.

79. Rahni, M.A.N.; Giaciliana, N.; Guilbault, G.G., Anal. Chem., 1986, 58, 523.

80. Elion, G., Fed. Proc. Fed. Amer. Soc. Exp. Biol., 1967, 26, 898.

81. Angel, J.E., In "Physician Desk Reference"; Medical Economic Company, Inc.: Oradell, N.J., 1983.

82. Jonkers, R.E.; Oosterhuis, B.; Ten Berge, R.J.M.; Van Boxtel, C.J., J. Chromatogr., 1982, 233, 249.

83. Finkel, J.M., Anal. Biochem., 1967, 21, 362.

84. Wong, P.C.P.; Maddocks, J.L., J. Chromatogr., 1978, 150, 491.

85. Floberg, S.; Hartvig, P.; Lindstrom, B.; Lonnerholm, G.; Odlind, B., J. Chromatogr., 1981, 225, 73.

86. Tsutsumi, K.; Otsuki, Y.; Kinoshita, T., J. Chromatogr., 1982, 231, 393.

87. Walsh, C., "Enzymatic Reaction Mechanism"; W.H. Freeman and Company: San Francisco, 1978.

88. Elving, P.J.; Schmakel, C.O.; Santhanam, K.S., CRC Crit. Rev. Anal. Chem., 1976, 6, 1.

89. Jaegfeldt, H., J. Electroanal. Chem., 1980, 110, 295.

90. Moiroux, J.; Elving, P.J., Anal. Chem., 1978, 50, 1056.

91. Gorton, L.; Johansson, G., J. Electroanal. Chem., 1980, 113, 151.

92. Gorton, L.; Torstensson, A., J. Electroanal. Chem., 1981, 130, 199.

93. Tse, D.C.S.; Kuwana, T., Anal. Chem., 1978, 50, 1315.

94. Massey, V.; Brumby, P.E.; Komai, H.J., J. Biol. Chem., 1969, 244, 1682.

95. Hille, R.; Massey, V., In "Molybdenum Enzymes"; Spiro, T.G., Ed.; John Wiley and Sons: New York, 1985.

96. Srivastava, S.K.; Krishnan, P.S., Biochem. J., 1962, 85, 33.

97. Suguira, M.; Yamamura, H.; Hirano, K.; Sasaki, M.; Morikawa, M.; Tsuboi, M., Chem. Pharm. Bull., 1979, 27, 2003.

98. Pietta, P.G.; Calatroni, A.; Agnellini, D.; Pace, M., Prep. Biochem., 1982, 12, 341.

99. Chiriboga, J., Biochem. Biophys. Res. Comm., 1963, 11, 277.

100. Metzger, R.P.; Wilcox, S.S.; Wick, A.N., J. Biol. Chem., 1965, 240, 2767.

101. Strecker, H.J.; Korker, S., J. Biol. Chem., 1952, 196, 769.

102. Brink, N.G., Acta Chem. Scand., 1953, 7, 1081.

103. Metzger, R.P.; Wilcox, S.S.; Wick, A.N., J. Biol. Chem., 1964, 239, 1769.

104. Kissinger, P.T.; Heineman, W.R., Eds., "Laboratory Techniques in Electroanalytical Chemistry"; Marcel Dekker: New York, 1984.

105. Nicholson, R.S.; Shain, I., Anal. Chem., 1964, 36, 706.

106. Bard, A.J.; Faulkner, L.R., "Electrochemical Methods"; John Wiley and Sons: New York, 1980.

107. Melby, L.R., Can. J. Chem., 1965, 43, 1448.

108. Blaedel, W.J.; Kissel, T., Anal. Chem., 1972, 44, 2109.

109. Allen, P.M.; Hill, H.A.O.; Oliver, B.N.; Walton, N.J., J. Am. Chem. Soc., 1984, 106, 921.

110. Armstrong, F.A.; Hill, H.A.O.; Oliver, B.N.; Walton, N.J., J. Am. Chem. Soc., 1984, 106, 921.

111. Harmer, M.A.; Hill, H.A.O., J. Electroanal. Chem., 1985, 189, 229,

112. Hill, H.A.O.; Page, D.J.; Walton, N.J.; Whitford, D., J. Electroanal. Chem., 1985, 187, 315.

113. Miyawaki, O.; Wingard, L.B., Biotechnol. Bioenger., 1984, 26, 1364.

114. Ikeda, T.; Katasho, I.; Kamei, M.; Senda, M., Agric. Biol. Chem., 1984, 48, 1969.

115. Ianniello, R.M.; Lindsay, T.J.; Yacynych, A.M., Anal. Chem., 1982, 54, 1098.

116. Blaedel, W.J.; Jenkins, R.A., Anal. Chem., 1974, 46, 1952.

117. Loach, P., In "Handbook of Biochemistry and Molecular Biology, 3rd ed., Physical and Chemical Data, Vol. 1," Fasmer, G.D., Ed., CRC Press: Cleveland, 1976, p. 126.

118. Owens, J.L.; Marsh, H.A.; Dryhurst, G., J. Electroanal. Chem., 1978, 91, 231.

119. Castner, J.F.; Wingard, L.B., Biochemistry, 1984, 23, 2203.

120. Albery, W.J.; Bartlett, P.N., J. Electroanal. Chem., 1985, 194, 211.

121. Chalmers, A.H.; Knight, P.R.; Atkinson, M.R., Aust. J. Exp. Biol. Med. Sci., 1969, 47, 263.

122. Greenlee, L.; Handler, P., J. Biol. Chem., 1964, 239, 1090.

123. Levine, I.N., "Physical Chemistry," MacGraw-Hill: New York, 1978, pp. 518-521.

124. Gough, D.A.; Leypoldt, J.K., Anal. Chem., 1979, 51, 439.

125. Gough, D.A.; Leypoldt, J.K., J. Electroanal. Chem., 1980, 127, 1278.

126. Mell, L.D.; Maloy, J.T., Anal. Chem., 1975, 47, 299.

127. Devlin, T.M., "Textbook of Biochemistry with Clinical Correlations," John Wiley and Sons: New York, 1986.

128. Childs, W.V.; Maloy, J.T.; Keszthelyi, C.P.; Bard, A.J., J. Electroanal. Chem., 1971, 118, 874.

129. Dryhurst, G., "Electrochemistry of Biological Molecules," Academic Press: New York, 1977.

130. Deakin, M.R.; Kovach, P.M.; Stutts, K.J.; Wightman, R.M., Anal. Chem., 1986, 58, 1474.

131. Kovach, P.M.; Ewing, A.G.; Wilson, R.L.; Wightman, R.M., J. Neurosci. Meth., 1984, 10, 215.

132. Dayton, M.A.; Ewing, A.G.; Wightman, R.M., Anal. Chem., 1980, 52, 2332.

133. Michael, A.C.; Justice, J.B., Anal. Chem., 1987, 59, 405.

134. Tse, D.C.S.; McCreery, R.L.; Adams, R.N., J. Med. Chem., 1976, 19, 37.

BIOGRAPHICAL SKETCH

Kevin McKenna was born on December 15, 1952, in Teaneck, New Jersey. He attended Northern Valley Regional High School in Demarest, New Jersey, and graduated in June, 1970. In 1972, he was drafted into the United States Army and spent 2 years working in the Pathology Department of Darnell Army Hospital in Killeen, Texas. After being honorably discharged, he accepted a position in the Pathology Department of York Hospital in York, Pennsylvania, where he worked for 8 years. During this time, he attended York College of Pennsylvania and York Hospital School of Medical Technology. He graduated in May, 1981, with a Bachelor of Science degree in medical technology.

In 1983, he was accepted into the graduate chemistry program at the University of Florida in Gainesville, Florida. He joined the research group of Dr. Anna F. Brajter-Toth and expects to formally receive his Doctor of Philosophy degree in the area of analytical chemistry in December, 1987.

I certify that I have read this study and that in my opinion it conforms to acceptable standards of scholarly presentation and is fully adequate, in scope and quality, as a dissertation for the degree of Doctor of Philosophy.

Anna Brajter-Toth, Chairperson
Assistant Professor of Chemistry

I certify that I have read this study and that in my opinion it conforms to acceptable standards of scholarly presentation and is fully adequate, in scope and quality, as a dissertation for the degree of Doctor of Philosophy.

James Winefordner
Graduate Research Professor of Chemistry

I certify that I have read this study and that in my opinion it conforms to acceptable standards of scholarly presentation and is fully adequate, in scope and quality, as a dissertation for the degree of Doctor of Philosophy.

Charles M. Allen, Jr.
Professor of Biochemistry and Molecular Biology

This dissertation was submitted to the Graduate Faculty of the Department of Chemistry in the College of Liberal Arts and Sciences and to the Graduate School and was accepted as partial fulfillment of the requirements for the degree of Doctor of Philosophy.

December, 1987

Dean, Graduate School